Quaternary Research (2019), **91**, 265–288.

doi:10.1017/qua.2018.61

Late Pleistocene records of speleothem stable isotopic compositions from Pinnacle Point on the South African south coast

Kerstin Braun[a,b,c]*, Miryam Bar-Matthews[a], Alan Matthews[b], Avner Ayalon[a], Richard M. Cowling[d], Panagiotis Karkanas[e], Erich C. Fisher[c], Kelsey Dyez[f], Tami Zilberman[a], Curtis W. Marean[c,d]

[a]Geological Survey of Israel, Jerusalem, Israel
[b]Fredy and Nadine Herrmann Institute of Earth Sciences, Hebrew University of Jerusalem, 91904 Jerusalem, Israel
[c]Institute of Human Origins, School of Human Evolution and Social Change, Arizona State University, Tempe, Arizona 85287, USA
[d]African Centre for Coastal Palaeoscience, Nelson Mandela University, Port Elizabeth, South Africa
[e]The Malcolm H. Wiener Laboratory for Archaeological Science, American School of Classical Studies, Athens, Greece
[f]Lamont-Doherty Earth Observatory, Columbia University, Palisades, New York, USA

(Received January 8, 2018; Accepted May 24, 2018)

Abstract

Highly resolved, well-dated paleoclimate records from the southern South African coast are needed to contextualize the evolution of the highly diverse extratropical plant communities of the Greater Cape Floristic Region (GCFR) and to assess the environmental impacts on early human hunter-gatherers. We present new speleothem stable oxygen and carbon isotope ratios ($\delta^{18}O_c$ and $\delta^{13}C$) from two caves at Pinnacle Point, South Africa, covering the time between 330 and 43 ka. Composite $\delta^{18}O_c$ and $\delta^{13}C$ records were constructed for Staircase Cave and PP29 by combining all stable isotope analyses into a single time series and smoothing by a 3-point running mean. $\delta^{18}O_c$ and $\delta^{13}C$ values record changes in rainfall seasonality and the proportions of C3 and C4 plants in the vegetation, respectively. We show that in general increased summer rainfall brought about a wider spread of C4 grasses and retreat of the C3 plant–dominated GCFR communities. The occurrence of summer rainfall on the southern coast of South Africa was linked to total rainfall amounts in the interior region through tropical temperate troughs. These rainfall systems shifted the southern coastal climate toward more summer (winter) rainfall when precession was high (low) and/or the westerlies were in a northern (southern) position.

Keywords: South Africa; Speleothem; Oxygen isotopes; Carbon isotopes

INTRODUCTION

The geographic location of southern Africa at the confluence of temperate and tropical/subtropical climatic systems (Schulze, 1972) and the Agulhas and Benguela Currents (Lutjeharms, 2006) leads to spatially complex modern climatic conditions. Within the context of the complexity and variability of climate conditions, the South African south coast is a key region for research on understanding the origins of modern humans (e.g., Marean et al., 2014; Wadley, 2015) as well as research in the highly diverse Greater Cape Floristic Region (GCFR; e.g., Allsopp et al., 2014). In order to analyze the effects of climate variations on our modern human ancestors and the vegetation dynamics and diversification in the region, we need to better understand the past climatic variability at this crossroad of atmospheric and oceanic circulation systems.

An outstanding feature of the South African climate is the seasonality of its rainfall distribution (Fig. 1a). The southwest of the country is dominated by Mediterranean-type winter rainfall, whereas the east and northeast get most of their rainfall during the summer. Our study site at Pinnacle Point on the south coast is located in the transition region between winter and summer rainfall, and rain may fall year-round (Fig. 1a). The rainfall season is determined by atmospheric interactions between the temperate westerlies, the subtropical anticyclones, and the tropical easterlies (Tyson and Preston-Whyte, 2000; Engelbrecht et al., 2015). The main rain-bearing systems on the south coast are ridges of the South Atlantic Anticyclone to the south of South Africa, which lead to advection and stratiform rainfall on the south coast, and the tropical temperate troughs that form when a continental heat low (or thermal low) links up with the westerlies to form convective cloud bands (Engelbrecht et al., 2015). A recent

*Corresponding author at: Institute of Human Origins, School of Human Evolution and Social Change, Arizona State University, P.O. Box 874101, Tempe, Arizona 85287, USA. E-mail address: kbraun2@asu.edu (K. Braun).

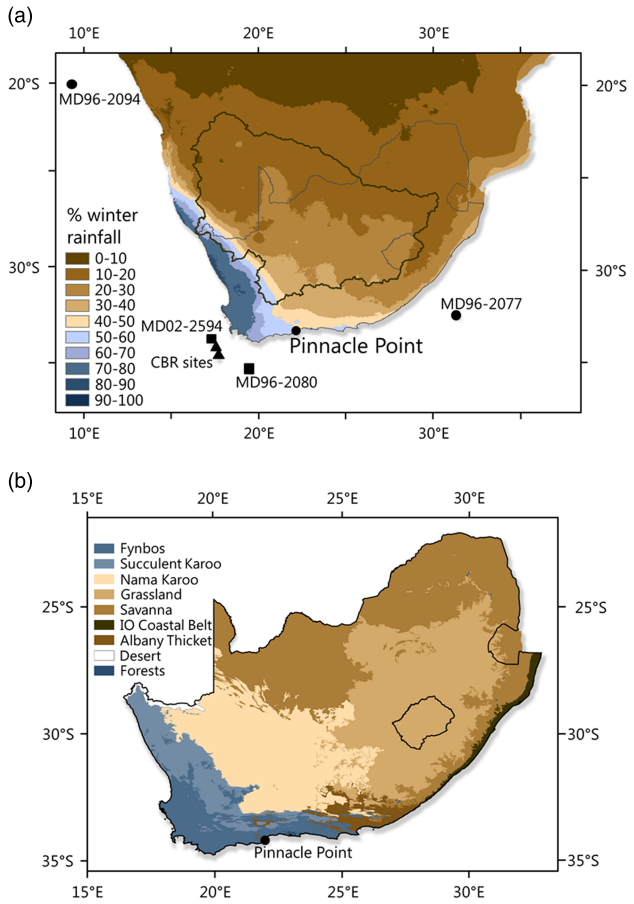

Figure 1. (color online) Maps of South Africa and surroundings. (a) Locations of Pinnacle Point and sediment cores used in analyses (dots for cores MD96-2094 [Stuut et al., 2002] and MD96-2077 [Bard and Rickaby, 2009]; squares for sites MD02-2594 and MD96-2080 [Martínez-Méndez et al., 2010]; triangles for sites of the Cape Basin Record [CBR; Peeters et al., 2004]); shading shows percentage of winter rainfall (legend in graph). The thick black outline delineates the catchment of the Orange River. (b) Distribution of vegetation biomes (Mucina and Rutherford, 2006), the Greater Cape Floristic Region combines the fynbos, succulent karoo, and Albany thicket biomes (Bergh et al., 2014).

study of the rainfall isotopic composition in the year-round rainfall region indicates that considerable changes of rainfall $\delta^{18}O$ ($\delta^{18}O_p$, ~ 5‰) are related to seasonal variations in synoptic conditions (Braun et al., 2017).

Present-day vegetation distribution in South Africa is closely tied to the seasonality and amount of rainfall. Fynbos, the megadiverse biome dominated by C3 plants, is mainly located in the southwestern winter rainfall region but also extends along the south coast into the year-round rainfall region (Fig. 1). As the proportion of summer rainfall increases on a west-to-east transect along the south coast, so does the fraction of C4 grasses in the vegetation (Vogel et al., 1978; Cowling, 1983). Toward the interior, total rainfall amounts decrease and fynbos communities are replaced by succulent karoo (Mucina and Rutherford, 2006), rich in crassulacean acid metabolism (CAM) plants. Together, the fynbos, succulent karoo, and subtropical thicket biomes are referred to as the GCFR (Allsopp et al., 2014). Given its extratropical location, the GCFR has extraordinarily high levels of plant and invertebrate diversity and endemism (Cowling et al., 1992; Goldblatt and Manning, 2002; Colville et al., 2014). However, this diversity is not equally distributed across the GCFR; the western, winter rainfall and C3–dominated areas have about double the number of species compared with the less seasonal rainfall region along the south coast (Cowling and Lombard, 2002). It has been suggested that this diversity is a response to differential environmental stability during the Quaternary, whereby eastern regions experienced stronger environmental fluctuations and therefore greater rates of GCFR lineage extinction than areas farther west (Cowling, 1983; Cowling and Lombard, 2002; Cowling et al., 2009).

A commonly accepted hypothesis for climate change in southern Africa on glacial-interglacial timescales suggests that increases in polar ice volume during glaciations led to a northward shift of the westerlies and increases in the spatial extent of the winter rainfall region (Van Zinderen Bakker, 1976, 1983), while the summer rainfall region experienced extended droughts (Van Zinderen Bakker and Illies, 1978; Van Zinderen Bakker, 1983). Considering the high spatial complexity of present-day climate, it is, however, not surprising that a growing number of climate reconstructions from different regions across southern Africa show considerable discrepancies (e.g., Scott et al., 2012; Chevalier and Chase, 2015).

Records of speleothem oxygen and carbon stable isotope ratios ($\delta^{18}O_c$, $\delta^{13}C$) are among the most powerful proxies for terrestrial climate change. Speleothem growth history can be directly and precisely dated using U-series disequilibrium dating (e.g., Hellstrom and Pickering, 2015). $\delta^{18}O_c$ values are influenced by the temperature at the cave site and by the $\delta^{18}O$ of the cave water, which reflects rainwater and fractionation processes in the water cycle (e.g., Gascoyne et al., 1980; McDermott, 2004). $\delta^{13}C$ values of speleothems in areas where C3 and C4 plants overlap primarily depend on their relative abundances in the vegetation above the cave (Dorale et al., 1992, 1998; Bar-Matthews et al., 1997; Denniston et al., 2001; Hopley et al., 2007). In the southern South African region, a pioneering carbon and oxygen stable isotope study at Cango Cave by Talma and Vogel (1992) revealed the potential of cave speleothems to record temperature change and rainfall variations, as well as the composition of the vegetation. Bar-Matthews et al. (2010) reconstructed past climate conditions using speleothems from Crevice Cave at Pinnacle Point. Their work showed that between 90 and 53 ka, periods of cool climate are generally associated with increased summer rainfall and a spread of C4 vegetation (Bar-Matthews et al., 2010).

The coastal cliffs at Pinnacle Point indeed represent a uniquely important environment for the study of past climates. The caves and rock shelters in these cliffs contain

https://doi.org/10.1017/qua.2018.61 Published online by Cambridge University Press

well-preserved archaeological deposits that have provided abundant evidence for hunter-gatherer adaptations in the middle and late Pleistocene (Marean et al., 2007; Brown et al., 2009, 2012; Jerardino and Marean, 2010; Karkanas et al., 2015; Wilkins et al., 2017). Taken together, the archaeological occupations date from ~160 to 50 ka (Marean et al., 2014), thus covering what is thought to be the formative period of the modern human lineage in Africa (Marean, 2015; Wadley, 2015). It is widely recognized that hunter-gatherer adaptations are strongly linked to climate and environmental change, and a major motivation of this study is to provide a long and well-dated climate record to help contextualize modern human origins in this region.

This study extends the Pinnacle Point speleothem $\delta^{18}O_c$ and $\delta^{13}C$ record to cover the interval between 330 and 43 ka. Despite several hiatuses in speleothem deposition, the extended record covers both interglacial and glacial conditions and thus allows us to assess the relative impacts of drivers of glacial-interglacial climate change. We explore different environmental parameters that may influence the $\delta^{18}O_c$ and $\delta^{13}C$ of speleothems at Pinnacle Point and compare our record with reconstructions of temperatures in Antarctica, sea surface temperature (SST) in the Agulhas Current region of the southwest Indian Ocean, a proxy for river runoff from the Orange River, and a proxy for shifts of the location of the subtropical convergence (STC) south of South Africa. This comparison allows us to present a new hypothesis on the effect of orbital scale changes in atmospheric pressure systems on climate in South Africa. Finally, we compare the climatic change indicated by our new proxy record with other proxies from the South African south coast and evaluate the impact of the environmental variations on human hunter-gatherers and GCFR plant communities.

Regional setting of the study

Pinnacle Point (34°12.47′S, 22°5.37′E; Fig. 1) is a coastal headland located 10 km west of the city of Mossel Bay. Caves and rock shelters are common in the steep coastal cliffs in the area.

Present-day climate

The average annual rainfall amount at Cape St. Blaize weather station at Mossel Bay (~6 km east of Pinnacle Point) is 330 mm, and annual average temperature is 17.5°C (National Climatic Data Center, National Oceanic and Atmospheric Administration, 2016). Seasonal temperature variations are low (~ 6°C difference between monthly average in February and July). Rainfall seasonality along the Cape south coast is moderate with all 12 months of the year contributing 5% or more to the long-term annual average (Engelbrecht et al., 2015). The isotopic composition of rainfall ($\delta^{18}O_p$) varies seasonally by ~5‰, depending on the shifts in synoptic conditions and changes in the contribution from stratiform and convective rainfall (Braun et al., 2017).

Regional environment and cave formation

The coastal cliffs at Pinnacle Point consist of the coarse quartzitic sandstones of the Skurweberg Formation (Paleozoic; Table Mountain Sandstone Group [TMS]), which contain fault breccias (Theron et al., 1989). Repeated sea level variations and wave action created caves and rock shelters by eroding these fault breccias. During periods of lowered sea levels, dunes formed on the exposed continental shelf and frequently sealed the cave sites as they migrated toward the cliffs. Unlithified dunes, eolianites, and calcretes assigned to the Bredasdorp Group (Klein Brak and Waenhuiskrans Formations; Pleistocene; Malan, 1990) are ubiquitous at Pinnacle Point, cemented to the cliffs, and across the landscape on top of the TMS. Speleothem and tufa formations are common in the caves with carbonate sources in the eolianites, calcarenites, and calcretes of the Bredasdorp Group.

The unusual development history of the caves in a quartzite host rock with closure by dunes leads to several possible complications for speleothem formation and stable isotopic equilibrium. In typical karstic caves, speleothem deposition in isotopic equilibrium is likely in poorly ventilated chambers where relative humidity and CO_2 concentration in the cave air are high (McDermott, 2004; Lachniet, 2009). However, in the small wave-cut caves at Pinnacle Point, ventilation is determined by the thickness and degree of cementation of the closing dune. During times when the cave is open, the deposition of tufa rather than speleothems is likely. Speleothem deposition may occur, however, when the cave has a small opening or is sealed by a thin dune cover with limited air circulation. Fluctuating CO_2 concentrations and humidity in the cave air can lead to fast CO_2 degassing or evaporation of drip water, respectively, which may result in kinetic isotope effects during speleothem formation. The more frequent and rapid shifts between open and closed conditions in the quartzite caves compared with typical karstic caves also lead to the formation of smaller speleothem deposits (closed cave) interbedded with layers of sand and tufa (open conditions). We address questions of the establishment of isotopic equilibrium by employing a combination of repetition tests, Hendy tests (Hendy, 1971), and petrographic analyses to identify an overall climatic signal in the stable isotopic records. Details of these tests are given in the "Materials and Methods."

The primary vegetation above the cliffs is limestone fynbos, a vegetation type dominated by C3 shrubs and rich in endemic species. Below the cliffs, strandveld and thicket, also C3-dominated vegetation types, prevail (Willis et al., 1996; Mucina and Rutherford, 2006). C3 and C4 grasses occur in roughly equal proportions in both vegetation types but form a relatively minor component. However, in renosterveld and some of the fynbos vegetation types to the interior of the study site, the grass component is sometimes high with C3 species (*Capechola, Pentemeris*) dominant on pole-facing slopes and C4 species on equator-facing slopes (Cowling, 1983).

https://doi.org/10.1017/qua.2018.61 Published online by Cambridge University Press

MATERIALS AND METHODS

Sampling

Speleothem samples were taken from two sites at Pinnacle Point: Staircase Cave and PP29, located 130 and 250 m west, respectively, of Crevice Cave studied by Bar-Matthews et al (2010). Both sites were wave cut and intermittently closed by coastal dunes, allowing for speleothem deposition (Bar-Matthews et al., 2010; Marean et al., 2010). PP29 is now an open cave, and vandalism has caused considerable damage to its deposits. Speleothem sampling included specimens from different parts of the cave to ensure a comprehensive coverage of all depositional phases at the highest possible resolution. Pieces of stalagmites, stalactites, and flowstones were cut using a combination of an angle grinder, core drill, diamond-bladed circular saw, and diamond-bladed chain saw. Staircase Cave is a collapsed cave, now only represented by remnants of clastic cave sediments and speleothems plastered to the cliff. Samples from Staircase Cave were drilled with a core drill into exposed flowstone and cut from edges of flowstones with an angle grinder, and some were removed from a crevice or pocket that had formed within the cave sediments.

All specimens were cut in half along their main growth axis with a diamond saw, and archives kept in South Africa. Aliquots for dating and stable isotope analyses were drilled from the other half.

U-series disequilibrium dating

U-series disequilibrium dating measurements were done at the Geological Survey of Israel (GSI) using procedures described by Vaks et al. (2006, 2010) and Grant et al. (2012). Aliquots for dating were drilled across speleothem samples following the growth laminae. Between 0.2 and 0.3 g of the speleothem material was drilled for each aliquot using a hand drill equipped with 0.8–4 mm diameter diamond drill bits. The calcite powder was dissolved in 7N HNO_3. Detrital material was separated in a centrifuge (10 minutes at 4000 rpm) and treated additionally with HNO_3 and HF. For calibration, a ^{229}Th + ^{236}U spike was added to all aliquots, which were then loaded into minicolumns that contained 2 mL Bio-Rad AG 1-X8 200–400 mesh resin. Thorium was eluted with 6N HCl, and uranium with 1N HBr. The two solutions were evaporated to dryness and dissolved in 5 mL and 2 mL of 0.1N HNO_3, respectively. Measurements were carried out using a multicollector inductively coupled plasma mass spectrometer (MC-ICP MS; Nu Instruments Ltd., UK) equipped with 12 Faraday cups and three ion counters. The aliquots were introduced to the MC-ICP MS through an Aridus microconcentric desolvating nebulizer sample introduction system. The instrumental mass bias was corrected for (using an exponential equation) by measuring the $^{235}U/^{238}U$ ratio and correcting with the natural value (137.88). The calibration of ion counters relative to Faraday cups was performed using several cycles of measurement with different collector configurations for each individual analysis. Age determination was possible because of the accurate determination of ^{234}U and ^{230}Th concentrations by isotope dilution analysis using the ^{236}U–^{229}Th spike. Uranium standard CRM 112A was analyzed every eight uranium samples. Values of half-lives for ^{230}Th and ^{234}U were taken from Cheng et al. (2013a). Concentrations of detrital thorium (represented by ^{232}Th) were between 1.1 and 153 ppb in PP29 and 0.2 to 254 ppb in Staircase Cave. Only one dating sample from Staircase Cave (46861-C1) had a higher concentration of ^{232}Th of 692 ppb and a low $^{230}Th/^{232}Th$ ratio (9.25) and therefore was corrected for detrital thorium. The corrected age assumes an initial $^{230}Th/^{232}Th$ atomic ratio of $4.4 \pm 2.2 \times 10^{-6}$, the value of material in secular equilibrium with the bulk earth $^{232}Th/^{238}U$ ratio of 3.8. The results of uranium and thorium isotopic analyses and the calculated ages with errors are presented in Table 1.

Stable isotope analyses of oxygen and carbon

Stable isotopic analyses of the speleothem carbonate were done using the protocols described in Bar-Matthews et al. (1997, 2003). For the analysis of $\delta^{18}O_c$ and $\delta^{13}C$, aliquots of 1–2 mg were drilled from the cross section of the samples at intervals of about 0.5 mm along the growth axis of the speleothem using a hand drill equipped with a 0.8 mm diameter drill bit. About 600–700 µg of the aliquots was weighed and put into glass vials at room temperature. Vials were dried uncapped in an oven at 60°C overnight to remove excess moisture. The vials were balanced horizontally, with the carbonate powder in the bottom and a drop of dry phosphoric acid (100%) at the top and flushed with pure helium gas for 10 minutes. After the needles used for flushing were removed, the vials were turned to a vertical position to allow for the dissolution of the carbonate in the phosphoric acid. The isotopic composition of CO_2 generated by the reaction was measured in a Finnigan Gas Bench II extraction system attached to a ThermoFinnigan DELTA plus XD mass spectrometer with a CTC Analytics automatic sampler at the GSI. Values where measured relative to international Standard NBS 19 and are reported in per mil (‰) relative to Vienna Pee Dee Belemnite. Analytical reproducibility is better than 0.1‰ for $\delta^{18}O_c$ and $\delta^{13}C$.

Results of the stable isotopic analyses of individual samples are given in Supplementary Table 1.

Age model construction

The diversity of the sample material, together with occurrence of hiatuses and outlier ages, necessitated the combined application of two methods of age model construction: linear interpolation and the algorithm StalAge (Scholz and Hoffmann, 2011). Initially, StalAge age models were used to identify major outliers and to provide an error envelope in the form of its 95% confidence limits. At the same time, a linearly interpolated age model was

https://doi.org/10.1017/qua.2018.61 Published online by Cambridge University Press

Table 1. Speleothem ^{230}Th dating results. Samples with no depth value were taken in a different part of the speleothem as the isotopic record and are not used in age models. b2k, before the year 2000.

Sample name	Depth (mm)	Weight (mg)	^{238}U (ppb)	±	^{230}Th (ppt)	±	^{232}Th (ppt)	±	[^{234}U]/[^{238}U] (activity)	±	[^{230}Th]/[^{232}Th] (activity)	±	[^{230}Th]/[^{238}U] (activity)	±	Age (yr before the year 2000)	Corrected age (yr before the year 2000)
Staircase Cave																
46322-A	8	162.7	1184	1.0	37	0.08	2366	3.6	1.96	0.002	2893	8	1.89	0.005	214,505	2784
46322-A1	10	156.8	1358	1.5	30	0.04	21,732	70.2	1.48	0.002	260	1	1.36	0.002	206,826	2059
46322-A2	15	144.5	1586	1.5	33	0.14	12,988	43.3	1.40	0.002	483	3	1.29	0.006	214,578	5790
46322-A3	20.5	136.1	2206	2.0	47	0.10	9960	22.1	1.39	0.002	877	3	1.29	0.003	223,772	3405
46322-A4	25	113.5	2955	2.6	66	0.25	10,015	30.5	1.42	0.002	1228	6	1.36	0.005	236,798	5804
46322-A5	27	130.9	2314	3.0	54	0.13	18,946	56.5	1.50	0.001	531	2	1.42	0.004	226,247	3466
46322-B	47	117.8	1351	0.9	44	0.11	5929	11.8	1.84	0.002	1404	4	2.01	0.005	329,577	8039
46322-B1	45	210.6	1668	1.3	57	0.17	4098	10.5	1.84	0.002	2600	10	2.09	0.006	394,808	15,335
46322-B2	41.5	140.5	581	0.6	30	0.11	5042	13.5	2.84	0.005	1097	5	3.11	0.012	275,588	7219
46322-B3	37	134.8	1524	1.2	55	0.15	9201	18.9	2.10	0.002	1127	4	2.22	0.006	272,084	5462
46322-B4	32.5	164.4	1676	1.5	47	0.16	8252	19.4	1.69	0.002	1055	4	1.70	0.006	251,663	5938
46322-B5	29	161.8	1924	1.7	57	0.12	11,143	23.5	1.80	0.002	960	3	1.82	0.004	252,085	4434
46330-a	51	137.8	3578	4.9	85	0.27	5741	15.3	1.55	0.003	2781	12	1.46	0.005	220,420	5293
46330-A	3	144.4	3161	3.0	69	0.53	25,397	63.9	1.45	0.004	508	4	1.33	0.010	210,783	9423
46330-A1	74	188.3	3014	3.0	71	0.20	2698	7.2	1.54	0.003	4954	19	1.45	0.004	220,369	4649
46330-A2	68	165	3204	3.1	76	0.16	2434	6.3	1.55	0.006	5805	19	1.44	0.003	210,363	5623
46330-A3	63	139	3038	3.3	72	0.14	10,326	20.8	1.56	0.002	1308	4	1.45	0.003	213,299	2978
46330-A4	57	177.1	3158	3.6	74	0.16	12,604	20.0	1.55	0.004	1103	3	1.44	0.004	210,027	4204
46330-B	9	123	2998	5.0	66	0.23	4055	12.7	1.46	0.004	3035	14	1.34	0.005	210,989	5119
46330-B1	47.5	176.1	3325	6.0	79	0.29	3498	9.2	1.56	0.005	4217	19	1.45	0.006	212,191	5899
46330-B2	44	154.6	3551	4.8	84	0.24	3972	12.8	1.55	0.003	3942	17	1.44	0.005	212,352	4247
46330-B3	39	175.1	3847	4.9	86	0.24	4870	13.2	1.48	0.002	3313	13	1.37	0.004	213,216	4264
46330-B4	33	168.5	3655	4.1	82	0.18	3085	6.0	1.48	0.001	4953	14	1.37	0.003	213,382	2795
46330-B5	29.5	163	3539	3.2	56	1.04	2712	82.0	1.47	0.002	3857	137	0.97	0.018	108,067	6371
46330-B6	22	203.2	3890	5.4	86	0.37	3306	15.9	1.47	0.003	4883	31	1.36	0.006	212,649	5495
46330-B7	16	136.9	3784	4.1	83	0.28	4998	16.5	1.46	0.001	3124	15	1.35	0.005	211,568	4231
46330-E	3	253.4	1324	1.9	43	0.34	18,153	30.2	2.22	0.005	443	4	1.99	0.016	176,075	5968
46330-F	9	275	6951	6.1	206	2.34	253,914	571.9	1.97	0.003	152	2	1.81	0.021	191,563	10,274
46330-G	14	219	1245	1.0	29	0.09	24,834	71.9	1.58	0.002	217	1	1.42	0.004	193,324	2959
46330-H	22	272	1385	1.3	30	0.05	8348	14.7	1.48	0.002	682	2	1.34	0.003	203,168	2259
46861-A	5.5	327.7	975	1.0	31	0.15	612	1.9	2.16	0.003	9589	55	1.97	0.010	183,879	4152
46861-A1	7	239.3	821	0.6	25	0.09	406	2.1	2.03	0.001	11,484	71	1.86	0.006	188,974	2958
46861-A2	11	260.5	1387	1.7	30	0.19	943	1.9	1.44	0.002	5915	40	1.32	0.009	208,137	7200
46861-AA3	16	182.2	1975	1.5	40	0.08	3265	4.6	1.37	0.001	2288	6	1.24	0.003	204,494	2548
46861-AA4	22	160.1	2203	1.2	45	0.12	4998	12.9	1.37	0.001	1669	6	1.24	0.003	206,189	4124
46861-B	30	301.4	3353	4.1	73	0.23	1115	3.5	1.44	0.002	12,311	54	1.34	0.004	215,141	4834

Table 1. (*Continued*)

Sample name	Depth (mm)	Weight (mg)	^{238}U (ppb)	±	^{230}Th (ppt)	±	^{232}Th (ppt)	±	[^{234}U]/[^{238}U] (activity)	±	[^{230}Th]/[^{232}Th] (activity)	±	[^{230}Th]/[^{238}U] (activity)	±	Age (yr before the year 2000)		Corrected age (yr before the year 2000)
46861-B1	38	233.9	3444	5.1	73	0.52	1405	3.9	1.41	0.002	9682	74	1.29	0.009	212,827	8550	
46861-B2	46	272	1302	0.7	36	0.33	1507	3.1	1.72	0.002	4434	42	1.68	0.016	232,312	12,707	
46861-B3	55	292.6	603	0.3	26	0.16	1131	2.3	2.45	0.003	4302	27	2.64	0.016	273,430	10,450	
46861-C	62	208.7	1442	1.1	48	0.17	3900	12.7	1.91	0.002	2287	11	2.02	0.007	281,972	7415	
46861-C1	66	271.4	1132	0.8	34	0.23	691,975	1152.8	1.73	0.002	9	0	1.85	0.012	312,454	18,738	304,762
50100-A	13	202	1651	1.6	42	0.10	1512	3.2	1.72	0.002	5246	16	1.57	0.004	195,794	2517	
50100-B	22	290.1	1816	1.6	44	0.17	846	2.3	1.62	0.002	9708	46	1.48	0.006	199,942	4088	
50100-C	26	200	1941	2.0	43	0.20	2344	5.0	1.47	0.002	3448	17	1.36	0.006	211,810	5462	
50100-D	35	287	1752	2.6	49	0.20	1198	1.8	1.77	0.003	7689	33	1.72	0.007	225,165	5396	
50100-1	39.5	261.2	1226	0.6	37	0.10	8067	18.3	1.86	0.001	865	3	1.86	0.005	239,656	3723	
50100-2	29.5	329.3	2310	1.9	54	0.12	1296	2.7	1.53	0.001	7855	24	1.44	0.003	219,642	2856	
50100-3	6	316.8	1527	1.1	48	0.11	1516	3.2	2.07	0.002	5944	18	1.93	0.005	194,971	2227	
142819-A	3	185.6	744	0.8	32	0.08	14,561	23.6	3.39	0.003	411	1	2.63	0.007	130,176	1146	
142819-A0	7	176.7	706	0.3	29	0.06	6096	8.5	3.27	0.003	905	2	2.56	0.005	131,535	913	
142819-A1	9	183.6	1648	1.4	70	0.10	655	0.9	3.20	0.004	20,075	38	2.61	0.004	141,378	897	
142819-A1A	13.5	207	1295	1.3	40	0.06	1629	2.2	2.05	0.002	4546	9	1.87	0.003	185,746	1576	
142819-A2	18	187.5	1274	0.8	35	0.09	1526	2.5	1.80	0.002	4246	13	1.66	0.004	197,576	2722	
142819-A3	25	160.3	1474	1.4	33	0.06	804	1.5	1.48	0.002	7676	20	1.37	0.003	211,058	2590	
142819-A4	29.5	157.3	3013	2.1	69	0.13	637	1.0	1.50	0.001	20,367	49	1.41	0.003	221,553	2482	
142819-B	36	73.4	2270	1.6	52	0.18	8018	2.6	1.59	0.002	1224	4	1.41	0.005	185,884	3612	
142819-C	40	265.4	1518	1.2	44	0.21	4149	14.8	1.81	0.002	2004	12	1.79	0.009	234,321	6527	
142819-C0	44	193.7	547	0.3	19	0.04	2758	4.1	1.99	0.001	1285	3	2.12	0.005	282,311	4290	
142819-C1	48	197.8	587	0.3	21	0.04	1198	1.4	2.00	0.002	3287	7	2.19	0.004	314,563	6291	
142819-C2	54	233.3	581	0.4	20	0.03	1621	2.7	1.96	0.002	2327	6	2.12	0.004	303,996	6080	
142819-D	62	271.2	1024	0.8	34	0.14	2124	6.9	1.87	0.001	2968	16	2.01	0.009	304,814	9882	
142820-A	43	123.3	846	0.3	28	0.06	8198	9.4	1.87	0.001	647	2	2.05	0.005	323,638	6473	
142820-1	3	177.8	1783	2.5	60	0.20	13,266	47.8	2.35	0.005	848	4	2.06	0.008	167,455	2714	
142820-B	33.5	143.5	1525	0.7	44	0.07	2472	3.5	1.75	0.002	3299	7	1.75	0.003	244,855	2801	
142820-C	29	175.5	2785	2.9	64	0.11	1238	2.5	1.46	0.001	9728	26	1.41	0.003	244,877	3259	
142820-D	25	124.7	2332	1.1	48	0.10	617	1.0	1.37	0.002	14,603	39	1.26	0.003	216,513	3292	
142820-E	21	131.6	1963	1.4	41	0.07	1421	1.4	1.38	0.001	5358	10	1.27	0.002	214,698	2350	
142820-F	15.5	174	1241	0.9	27	0.05	219	0.5	1.47	0.002	23,348	63	1.35	0.002	209,255	2322	
142820-G	11.5	142.3	1064	0.9	29	0.08	579	1.3	1.86	0.002	9513	35	1.69	0.005	190,013	2722	
PP29																	
46745-A	69	94.7	1621	1.3	31	0.05	4694	49.2	1.77	0.001	1228	13	1.16	0.002	105,142	736	
46745-A1	54.5	236.2	1775	2.2	36	0.09	2724	4.6	1.82	0.002	2475	8	1.24	0.004	111,418	1202	
46745-A2	34	250.2	1232	1.4	28	0.05	2629	3.6	2.05	0.001	1995	5	1.39	0.003	109,489	729	
46745-A3	18.5	281.2	1444	1.6	29	0.06	1252	1.7	2.10	0.002	4275	11	1.21	0.003	85,887	598	

Table 1. (*Continued*)

Sample name	Depth (mm)	Weight (mg)	^{238}U (ppb)	±	^{230}Th (ppt)	±	^{232}Th (ppt)	±	[^{234}U]/[^{238}U] (activity)	±	[^{230}Th]/[^{232}Th] (activity)	±	[^{230}Th]/[^{238}U] (activity)	±	Age (yr before the year 2000)	Corrected age (yr before the year 2000)
46745-B	5	149.6	1094	0.5	19	0.06	3561	7.6	2.14	0.000	1021	4	1.09	0.003	71,802	783
46746-A	4	247.1	839	0.8	25	0.05	3959	8.1	3.05	0.001	1174	3	1.81	0.004	87,275	559
46746-A1	8.5	113.3	625	0.3	19	0.06	3855	9.6	3.03	0.000	936	4	1.88	0.006	93,183	799
46746-A2	16	121.8	652	0.4	18	0.03	5502	6.7	2.62	0.000	596	1	1.64	0.003	94,996	578
46746-A3	27	136.7	1051	0.5	27	0.06	3346	4.9	2.39	0.000	1533	4	1.60	0.004	105,102	781
46746-B	32	38.3	712	0.4	19	0.11	5448	18.1	2.51	0.000	652	5	1.62	0.010	99,519	1991
46746-B1	33.5	138.6	801	0.8	20	0.04	12,128	22.1	2.43	0.001	315	1	1.56	0.004	98,959	728
46746-B2	40	150.4	468	0.2	15	0.02	1944	2.3	2.94	0.000	1422	3	1.93	0.003	100,977	547
46746-B3	47.5	151.3	2102	1.7	48	0.06	1159	1.7	2.43	0.002	7748	15	1.40	0.002	84,486	470
46746-B4	55	174.4	988	0.7	22	0.04	1537	1.9	2.46	0.001	2704	6	1.37	0.002	81,261	449
46746-C	66	274	491	0.2	14	0.05	1989	6.2	3.18	0.000	1276	6	1.69	0.006	75,172	773
46746-D	72	161.4	573	0.3	13	0.03	1316	4.9	3.92	0.000	1896	8	1.42	0.003	46,438	266
46747-A	2	56.5	724	1.7	12	0.26	5704	55.5	3.11	0.002	399	9	1.02	0.022	41,531	2137
46747-B	0	71.6	321	1.1	18	0.29	18,297	237.6	4.16	0.001	186	4	3.46	0.057	143,527	8769
46747-C	21	34.9	1044	3.2	23	0.21	7482	45.1	3.03	0.003	590	6	1.38	0.013	61,315	1575
138862.1-A	3	216.4	785	0.6	17	0.05	2124	5.1	2.91	0.001	1489	6	1.32	0.004	61,207	465
138862.1-A1	12	224.1	4533	5.3	120	0.23	54,120	83.1	3.11	0.005	416	1	1.62	0.004	73,415	432
138862.1-A2	23	284.9	276	0.3	9	0.02	1103	2.0	3.78	0.000	1570	4	2.05	0.005	76,702	451
138862.1-A3	33	286.5	1151	0.8	26	0.04	3326	5.9	2.37	0.001	1464	4	1.38	0.002	86,446	461
138862.1-A4	47	254.7	1041	0.6	26	0.06	2479	4.3	2.56	0.001	1952	6	1.52	0.004	88,485	635
138862.1-B	58	268.4	1120	0.9	27	0.07	4992	28.0	2.46	0.001	1009	6	1.47	0.004	89,136	703
138862.1-C	0	184.3	2859	2.7	107	0.17	153,343	203.0	3.26	0.003	130	0	2.29	0.004	110,723	690
138862.2-A	22	178.8	1135	1.2	27	0.07	9616	22.1	2.50	0.001	523	2	1.45	0.004	85,036	667
138862.2-A1	27	216.4	1167	0.9	29	0.05	6528	10.0	2.51	0.001	826	2	1.51	0.003	90,098	582
138862-2-B	32	259.8	1036	1.1	26	0.07	3467	9.2	2.59	0.0002	1393	5	1.52	0.005	87,238	685
138862.2-B1	37	197.3	928	0.7	23	0.06	7647	14.2	2.63	0.001	574	2	1.55	0.004	87,127	679
138862.2-C	3	62.5	893	0.7	27	0.11	13,821	36.3	2.80	0.001	368	2	1.86	0.008	103,452	1278
138862.2-C1	8	128.9	1571	1.2	46	0.09	11,335	17.5	2.67	0.001	766	2	1.81	0.004	106,703	615
138862.2-D	24	166.8	2654	3.0	76	0.14	3660	6.5	2.55	0.003	3877	10	1.75	0.004	109,200	707
138862.2-D1	15	165	2466	3.1	69	0.14	4133	6.7	2.48	0.003	3126	8	1.71	0.004	110,425	843
142828-A	2	279.8	1262	0.9	17	0.06	3780	10.8	2.11	0.001	833	4	0.82	0.003	50,975	539
142828-A1	6	251.2	957	0.4	14	0.03	2103	2.1	2.01	0.000	1209	3	0.87	0.002	58,437	355
142828-A2	10	221.6	263	0.2	8	0.02	1091	1.7	2.92	0.000	1389	4	1.88	0.004	98,024	694
142828-A3	16	199.5	932	0.8	20	0.03	1986	3.0	1.95	0.001	1847	4	1.29	0.002	104,921	676
142828-A4	21	210.6	181	0.1	5	0.02	2795	7.3	2.80	0.000	368	2	1.86	0.008	103,452	1278
142828-A5	26	132.7	1967	1.4	38	0.08	2452	3.4	1.75	0.001	2891	7	1.18	0.003	109,856	884
142828-B	34	306.3	2468	2.6	46	0.08	2609	3.4	1.73	0.003	3276	7	1.13	0.002	105,420	726
142828-C	11	221.3	283	0.2	8	0.02	2090	5.0	2.69	0.000	703	2	1.70	0.004	95,994	646
142828-D	32	255.2	2268	2.7	43	0.13	1674	4.2	1.76	0.003	4840	19	1.17	0.004	107,654	1238

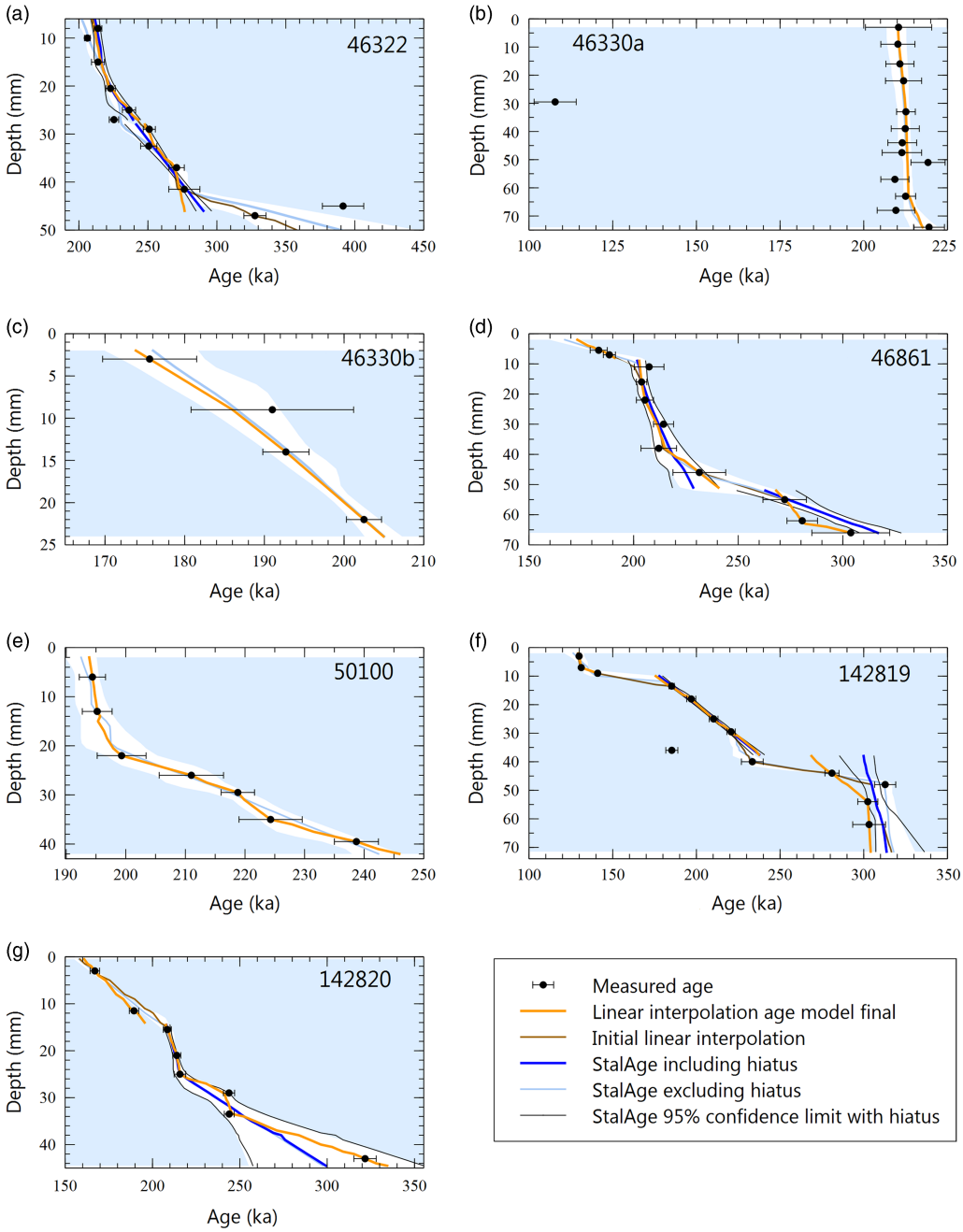

Figure 2. (color online) (a–g) Age-depth plots showing measured ages for samples from Staircase Cave and age models constructed by linear interpolation and using StalAge (Scholz and Hoffmann, 2011; legend is given in figure). White background indicates 95% confidence interval of initial StalAge age model (not accounting for hiatuses). Detailed description of age model construction for individual samples can be found in Supplementary Chapter 1. Linear interpolation age models generally overlap well with StalAge age models in sections where both methods could be applied.

constructed using all ages in stratigraphic order and assuming continuous growth. Sections of the samples in which the growth rates given by the initial age models were reduced by a factor of 10 compared with the rest of the sample were examined for evidence of hiatuses using petrographic criteria (variations of color, the presence of white laminae, sharp changes in isotopic values, and switches of the crystal fabric and growth habit in thin section; Supplementary Fig. 1). In cases where several indications for a hiatus were found, the sample was subdivided at the hiatus boundary into separate growth phases, and new linear interpolation and StalAge age models were constructed for the subsections of the sample. Continuously grown sections of speleothems generally show good agreement between linear interpolation and StalAge age models (Figs. 2 and 3), but variations in growth rate can bring about deviations between the StalAge and linear interpolation age models (e.g., Fig. 2d and f).

https://doi.org/10.1017/qua.2018.61 Published online by Cambridge University Press

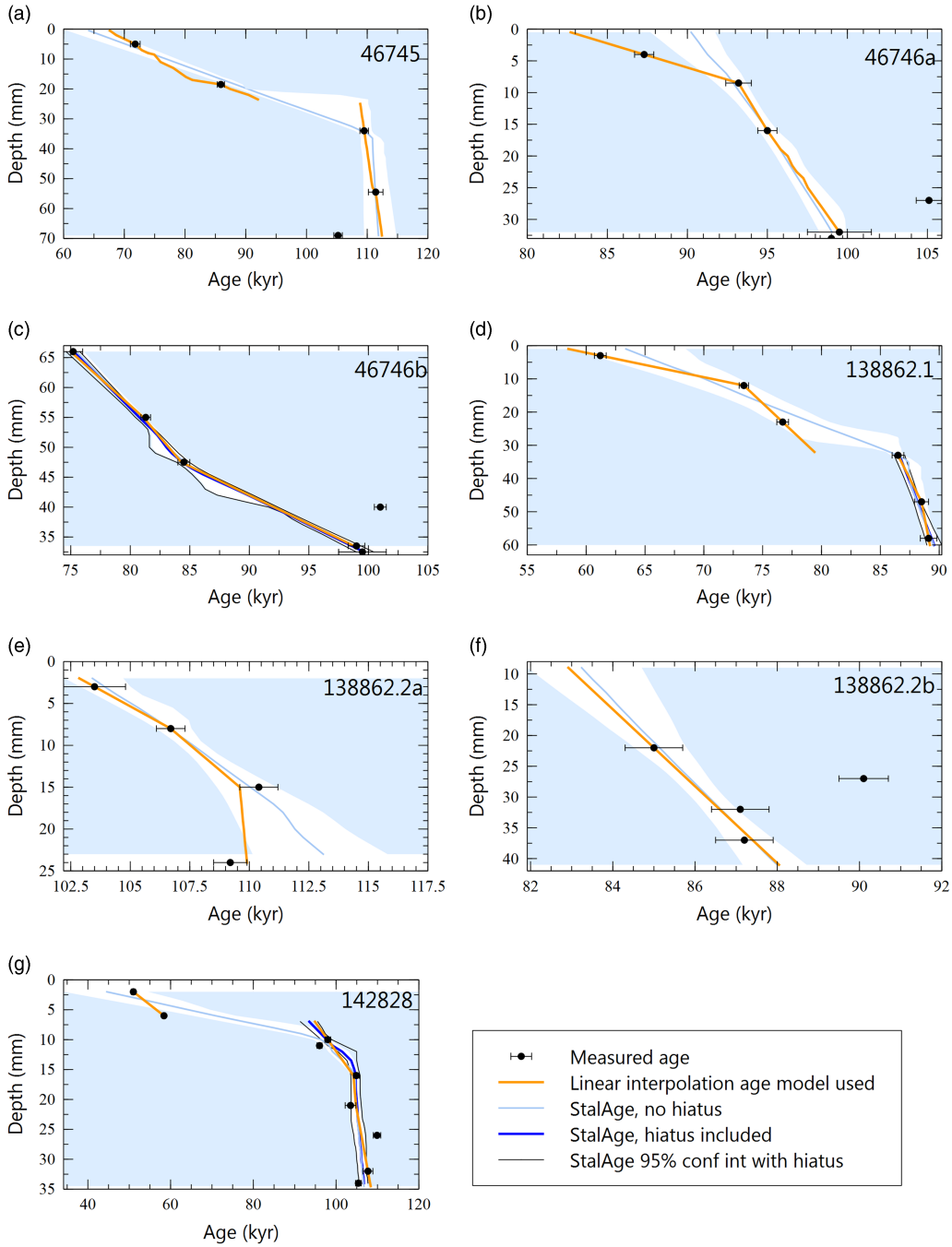

Figure 3. (color online) (a–g) Age-depth plots showing measured ages for samples from PP29 and age models constructed by linear interpolation and using StalAge (Scholz and Hoffmann, 2011; legend is given in figure). White background indicates 95% confidence interval of initial StalAge age model (not accounting for hiatuses). Detailed description of age model construction for individual samples can be found in Supplementary Chapter 1. Linear interpolation age models generally overlap well with StalAge age models in sections where both methods could be applied.

The subdivision into different growth intervals created subsections in some of the samples for which age modelling using StalAge was not possible; either they were only dated by two ages, or changes in growth rate within the section led to problems in the algorithm's check for outliers. We therefore constructed linearly interpolated age models for these sections of the samples, which usually were within the 95% confidence limit of the initial StalAge age models that did not account for hiatuses. Figures 2 and 3 show the final age model compared with StalAge age models for each of the samples. Individual samples and age models are described in Supplementary Chapter 1, and data are given in Supplementary Table 1.

Correlation of trends in the records

Statistical analyses of correlation between different time series were performed using the R software environment for statistical

https://doi.org/10.1017/qua.2018.61 Published online by Cambridge University Press

computing and graphics (R Core Team, 2017). To allow for the analysis of correlation between data sets, the different sets were smoothed using a spline interpolation following the methods described in Fritsch and Carlson (1980). We achieved this by applying the "splinefun" function of the "stats" package in R with the method "monoH.FC." In this manner, we created a monotone piecewise cubic interpolation function of the original data sets that could then be sampled at defined and equally spaced intervals using the "seq" function of the "base" R package. Resampling our speleothem $\delta^{18}O_c$ and $\delta^{13}C$ records at the same resolution and the same points in time as the relevant proxy records allowed us to calculate Pearson's correlation coefficients and *P* values using the "cor.test" function in R's "stats" package. Supplementary Figure 2 shows a comparison of the original data sets with spline functions sampled at 1 ka intervals for the Staircase Cave $\delta^{18}O_c$ values and the key proxy records referred to in this study (SST from sediment cores MD96-2080 and MD02-2594: Martínez-Méndez et al., 2010; relative sea level: Rohling et al., 2009; proportion of hemipelagic mud in core MD96-2094: Stuut et al., 2002). Values of Pearson's correlation coefficient (*r*) between –0.3 and +0.3 are considered "weak" correlation, values of –0.5 to –0.3 and 0.3 to 0.5 are "moderate", and values between –1 and –0.5 and from 0.5 to 1 are considered "strong". Significant correlation is generally assumed for *P* values below 0.01.

Because of the strong smoothing performed by the spline functions, the correlation coefficients represent only the compatibility of overall trends and cannot be interpreted in terms of a correlation of the actual measured data.

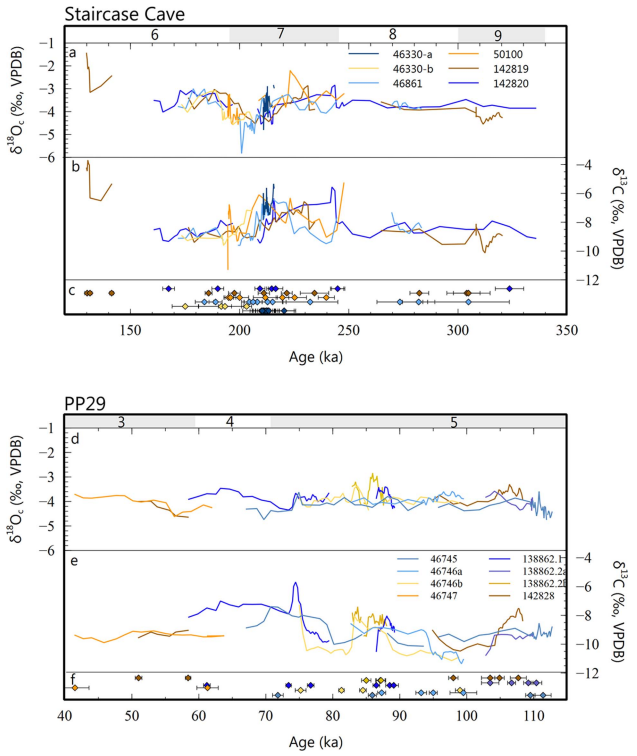

Figure 4. (color online) $\delta^{18}O_c$ and $\delta^{13}C$ of all samples from Staircase Cave (a, b) and PP29 (d, e). In panels c and f, measured age results with 2σ errors are shown. The different samples from the same cave site show good compatibility of $\delta^{18}O_c$ and $\delta^{13}C$ values and trends. Numbers at the top of the panels denote Marine Oxygen Isotope Stages. VPDB, Vienna Pee Dee belemnite.

RESULTS

Dating results

Ages used for the construction of age models in this study range between 329.6 ± 7.9 ka (46322-B) and 130.2 ± 1.1 ka (142819-A) for Staircase Cave and from 111.4 ± 1.2 ka (46745-A1) to 41.5 ± 2.1 ka (46747-a) for PP29. Out of the 104 age analyses performed on the samples from PP29 and Staircase Cave, 5 had 2σ errors above 5% of the age value, and the highest error was 6.0% of its respective age. Plots of the age against depth for all samples are shown in Figures 2 and 3. Images of the samples are shown in Supplementary Figures 3 and 4.

Fully comprehensive sampling of Staircase Cave was not feasible as a result of it being a collapsed site. It is therefore possible that the samples recovered from the excavated residual parts of the site do not represent the complete deposition cycle.

Tests of stable isotopic equilibrium

The formation history of the sea caves at Pinnacle Point raises concerns that kinetic, rather than equilibrium, isotope effects may be affecting $\delta^{18}O_c$ and $\delta^{13}C$, because it is unclear when the caves were fully closed or when they may have been partially ventilated. We therefore apply a combination of Hendy (1971) tests and repetition tests (Dorale and Liu, 2009) to assess the closeness to isotopic equilibrium deposition of the speleothem samples.

The two Hendy tests (Hendy, 1971) made on one sample from PP29 (138862.2) and one from Staircase Cave (142819) do not show correlation of $\delta^{18}O_c$ with $\delta^{13}C$ along single growth layers (Supplementary Fig. 5a) suggesting slow CO_2 degassing and carbonate deposition in isotopic equilibrium (Hendy, 1971). In addition, $\delta^{18}O_c$ values do not increase along the laminae (Supplementary Fig. 5b) showing that evaporation was not substantial (Hendy, 1971).

Correlation of $\delta^{18}O_c$ and $\delta^{13}C$ along the main growth axis of a speleothem may reflect kinetic isotope effects (Hendy, 1971; Mickler et al., 2006). Such correlation, however, can also be caused by environmental changes that lead to simultaneous variations of $\delta^{18}O_c$ and $\delta^{13}C$ (e.g., Dorale and Liu, 2009; Bar-Matthews et al., 2010). Three records from Staircase Cave (46330a, 50100, and 142819; Supplementary Fig. 6) and two records from PP29 (138862.2b and 142828; Supplementary Fig. 7) show strong and significant positive correlations between $\delta^{18}O_c$ and $\delta^{13}C$ ($r > 0.5$, $P < 0.01$).

For the repetition test, the stable isotopic records of coeval samples from the same cave or region are directly compared with each other. Although this test is emerging as a new standard for the assessment of isotopic equilibrium, speleothem studies rarely include more than two or three coeval

https://doi.org/10.1017/qua.2018.61 Published online by Cambridge University Press

samples (e.g., Boch et al., 2009; Stríkis et al., 2011; Cheng et al., 2013b; Kanner et al., 2014; Lachniet, 2015; Oster et al., 2015). Our study includes seven records from Staircase Cave and eight from PP29, all of which have highly variable resolutions and age uncertainties. Nevertheless, differences between $\delta^{18}O_c$ values of coeval samples are usually less than 1.0‰ (Fig. 4a and d). There also is a good overlap of the overall trends for the $\delta^{13}C$ values (Fig. 4b and e), suggesting that minor offsets between samples may be related to differences of the growth rate and age errors. In view of the good overlap for both isotopes, we assume that kinetic isotope effects represent a minor influence at Staircase Cave and PP29, at least for time intervals covered by several samples. Furthermore, we chose a method of composite record construction (described in the following section) that accounts for the minor differences between individual samples and smooths them into a record that represents overall environmental trends.

Composite record construction

We created composite records of stable isotopes at each site by chronologically merging records from all speleothems using the estimated ages given by each record's age model. Stable isotopic values were smoothed with a 3-point running mean to reduce local noise following a modified approach described by Williams et al. (2005). Because our speleothem samples often cover different time intervals and have variable resolutions, we did not adjust them to a common mean as done by Williams et al. (2005). We estimate the confidence intervals around the 3-point running mean of the $\delta^{18}O_c$ and $\delta^{13}C$ values by bootstrapping with replacement over 1000 iterations. We calculated the 5th and 95th percentiles for the $\delta^{18}O_c$ and $\delta^{13}C$ of the composite records and plotted them, along with the 3-point running mean and original values, in Figure 5. Periods with the greatest precision of isotope values were observed where the growth of multiple speleothems overlapped and where temporal resolution was highest, such as the period between 220 and 190 ka.

Staircase Cave

The composite stable isotopic record of Staircase Cave covers the period from 330 to 130 ka (Fig. 5a, Supplementary Table 2); it includes a total of 291 $\delta^{18}O_c$ and $\delta^{13}C$ analyses. There is no chronological overlap of the Staircase Cave record with those of PP29 and Crevice Cave (Bar-Matthews et al. 2010). $\delta^{18}O_c$ and $\delta^{13}C$ values of the smoothed record range mostly from –5.0‰ to –2.7‰ and from –9.8‰ to –6.2‰, respectively. A short interval at the transition between Marine Oxygen Isotope Stage (MIS) 6 and MIS 5 has exceptionally high values of $\delta^{18}O_c$ (–2.8‰ to –1.8‰) and $\delta^{13}C$ (–6.1‰ to –3.9‰).

In MIS 9 and 8 (330–250 ka), values of $\delta^{18}O_c$ generally show small variations between –4.4‰ and –3.4‰. $\delta^{13}C$ values mostly range between –9.8‰ and –7.8‰. At the transition from glacial MIS 8 into interglacial MIS 7, $\delta^{18}O_c$ and $\delta^{13}C$ increase from –3.8‰ to –3.2‰ and from –8.8‰ to –6.5‰, respectively (Fig. 5a, Supplementary Table 2). The $\delta^{18}O_c$ values in early MIS 7 (245–217 ka) are between –3.8‰ and –3.1‰ with a short peak of –2.7‰ between 226 and 223 ka. In late MIS 7 (217–206 ka), $\delta^{18}O_c$ values gradually decrease from –2.8‰ to –4.7‰, and they remain low (–4.2‰) until the beginning of MIS 6 (195 ka). Values of $\delta^{13}C$ show larger variability in early MIS 7 than in MIS 9 and MIS 8, between –9.3‰ and –6.2‰. In late MIS 7 (211–200 ka), $\delta^{13}C$ values gradually decrease from –6.2‰ to –9.1‰.

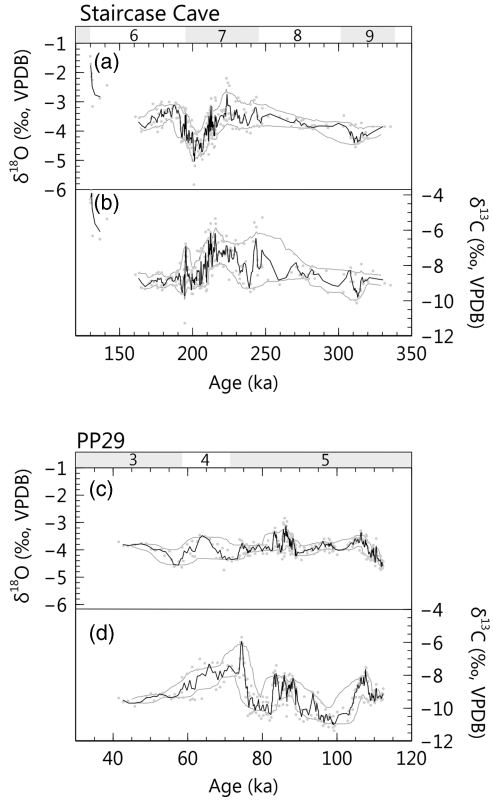

Figure 5. Three-point running mean composite $\delta^{18}O_c$ and $\delta^{13}C$ records of Staircase Cave (a) and PP29 (b) with 5th and 95th percentile confidence intervals constructed using 1000 iterations of bootstrapping with replacement. All individual isotope analyses are shown in gray. Numbers at the top of the panels denote Marine Oxygen Isotope Stages. VPDB, Vienna Pee Dee belemnite.

After the decrease in late MIS 7, and in the early part of MIS 6 (203–163 ka), $\delta^{13}C$ values mostly remain low and stable between –8.4‰ and –9.7‰. Values of $\delta^{18}O_c$ increase gradually from the low values in late MIS 7 (approximately –4.7‰) into early MIS 6 (–3.1‰ at 187 ka). $\delta^{18}O_c$ values are –3.7‰ at the onset of the hiatus in deposition at 163 ka. In the interval following the hiatus between 137 and 130 ka, both $\delta^{18}O_c$ and $\delta^{13}C$ have high values and show increasing trends ($\delta^{18}O_c$: –2.8‰ to –1.8‰; $\delta^{13}C$: –6.1‰ to –3.9‰). Because this interval is covered only by one sample, it may not reflect average conditions at the site and kinetic effects may be affecting these extraordinary values.

https://doi.org/10.1017/qua.2018.61 Published online by Cambridge University Press

PP29

The composite stable isotopic record of PP29 (Fig. 5b, Supplementary Table 2) covers the interval between 112 and 43 ka and is based on 280 isotopic analyses. $\delta^{18}O_c$ and $\delta^{13}C$ values vary from –4.6‰ to –3.1‰ and from –11.0‰ to –5.9‰, respectively.

In late MIS 5, between 112 and 74 ka, $\delta^{18}O_c$ in PP29 shows irregular variations, between –4.6‰ and –3.0‰. Values of $\delta^{13}C$ cyclically vary between –11.0‰ and –7.6‰ for most of late MIS 5, with high values (approximately –8.0‰) at 107 ka and 88–83 ka. The transition from MIS 5 into MIS 4 at ~ 76–74 ka is marked by a steep increase of the $\delta^{13}C$ values from –10.0‰ to –5.9‰ (Fig. 5b, Supplementary Table 2) and a less pronounced peak of the $\delta^{18}O_c$ record (–3.8‰). During MIS 4, $\delta^{18}O_c$ values gradually increase from –4.3‰ to –3.5‰, whereas $\delta^{13}C$ values remain high (between –8.2‰ and –7.2‰). At the transition from MIS 4 into MIS 3, $\delta^{18}O_c$ and $\delta^{13}C$ decrease from –3.5‰ (at 64 ka) to –4.6‰ (at 58 ka) and from –7.3‰ to –9.3‰, respectively. In early MIS 3, between 57 and 43 ka, $\delta^{18}O_c$ values increase from –4.5‰ to –3.8‰, whereas $\delta^{13}C$ remains stable (between –9.7‰ and –9.2‰).

DISCUSSION

Factors influencing the speleothem stable isotope records

Controls of speleothem $\delta^{18}O_c$ values

The main controls of $\delta^{18}O_c$ are the cave temperature and the $\delta^{18}O$ of cave water at the time of speleothem formation. Because of the dense fracture system in the host rock at Pinnacle Point, water infiltrates quickly (Karkanas and Goldberg, 2010), and cave water $\delta^{18}O$ thus most likely reflects the $\delta^{18}O_p$ of local rainfall without effects of evaporation.

Temperature has a dual impact on $\delta^{18}O_c$: an indirect effect attributable to the temperature dependence of fractionation between water vapor and raindrops in the atmosphere, and the direct effect attributable to the temperature dependence of fractionation between drip water and carbonate inside the cave. The temperature of a cave is close to the mean annual surface temperature of the region in which it is situated. However, resampled $\delta^{18}O_c$ values from Staircase Cave show no correlation with SST from the Cape Basin (cores MD02-2594 and MD96-2080; $r = 0.073$, $P = 0.35$; Figs. 1a and 6a; Martínez-Méndez et al., 2010). If oceanic temperatures are taken as a first approximation for terrestrial temperatures in the coastal region (see Bar-Matthews et al., 2003; Almogi-Labin et al., 2009, for the Mediterranean region), then changes in $\delta^{18}O_c$ are not correlated with land temperature variation. Some other factor must be overriding the temperature effect.

Variations of global sea level may affect $\delta^{18}O_c$ through changes in relative altitude of the cave and the distance to the sea. Both factors potentially decrease the $\delta^{18}O_p$ during phases of low sea level compared with sea level high stands (Rozanski et al., 1993; Poage and Chamberlain, 2001; Winnick et al., 2014). The overall trends of the smoothed $\delta^{18}O_c$ record from the longest continuous growth period at Staircase Cave (between 331 and 163 ka), however, show only a weak

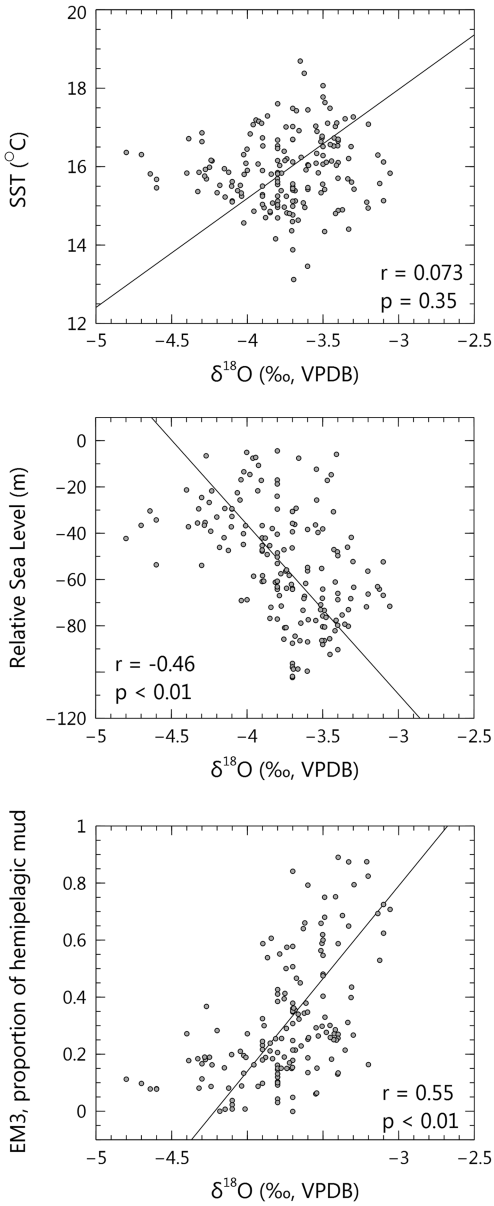

Figure 6. Scatter plots of the exponential spline smoothed and resampled record of $\delta^{18}O_c$ from Staircase Cave against the sea surface temperature (SST) records reconstructed using Mg/Ca ratios of *Globigerina bulloides* from sediment cores MD02-2594 and MD96-2080 (a; Martínez-Méndez et al., 2010); relative sea level (b; Rohling et al., 2009); and the river-derived sediment size fraction of core MD96-2094 (c; Stuut et al., 2002). Only the longest continuous growth period of speleothems at Pinnacle Point (between 328 and 163 ka) was included in these analyses. Data sets were resampled at 1 ka intervals. Regression lines were calculated using reduced major axis regression. EM3, end member 3; VPDB, Vienna Pee Dee belemnite.

https://doi.org/10.1017/qua.2018.61 Published online by Cambridge University Press

negative correlation with sea level ($r = -0.46$, $P < 0.01$; Fig. 6b; Rohling et al., 2009), implying that low $\delta^{18}O_c$ values are not associated with low sea levels and that there is a negligible effect of sea level change.

Globally, the most important factors influencing $\delta^{18}O_p$ are temperature (in temperate regions) and rainfall amount (in the tropics). Given its location between temperate and tropical climate regions, the complex patterns of rainfall seasonality across South Africa have a profound effect on $\delta^{18}O_p$. In Pretoria, in the summer rainfall region, $\delta^{18}O_p$ shows the correlation with rainfall amount that is characteristic for tropical rainfall (Braun et al., 2017). In contrast, in Cape Town, in the coastal Mediterranean climate region, there is only minor correlation of $\delta^{18}O_p$ with both temperature and rainfall amount (Bowen, 2008; Braun et al., 2017). Rainfall in the South African year-round rainfall region is a synoptically complex combination of tropical, subtropical, and temperate atmospheric pressure systems (Engelbrecht et al., 2015; Engelbrecht and Landman, 2016).

Modern rainfall sampling at Mossel Bay in the year-round rainfall region during a 4 yr period (2009–2012) when winter rainfall dominated interannual variability reveals similar low correlation between $\delta^{18}O_p$ and temperature/rainfall amount as at Cape Town (Braun et al., 2017). However, the amplitude of seasonal $\delta^{18}O_p$ variations is more than twice as high in Mossel Bay (4.8‰) than at Cape Town (2.2‰). Braun et al. (2017) attribute this larger amplitude to the seasonal variations in the complex synoptic conditions influencing precipitation in the year-round rainfall region. Temperate cold fronts, which are a major source for rain in the winter rainfall region, only contribute 5% of the rainfall on the south coast (Engelbrecht et al., 2015). More significant contributions are from ridges of the South Atlantic Anticyclone to the southwest of the continent (46%), tropical temperate troughs (28%), and troughs to the southeast of the continent (8%; Engelbrecht et al., 2015). Ridging anticyclones do not contribute much to seasonality, because they occur all year-round (Fig. 7a; Engelbrecht and Landman, 2016). Tropical temperate troughs peak in late summer (January–April, Fig. 7a) and are associated with strong convection (Fig. 7a; Todd and Washington, 1999; Engelbrecht and Landman, 2016). High-altitude condensation leads to high values of $\delta^{18}O_p$ of convective clouds, and large drop sizes prohibit isotopic equilibration with surrounding vapor as the drops fall (Aggarwal et al., 2016). Troughs to the southeast occur most frequently in the winter months (June–September, Fig. 7a; Engelbrecht and Landman, 2016) and mostly bring stratiform rainfall. The condensation altitude is lower in stratiform clouds, and the size of raindrops is smaller than in convective clouds; raindrops therefore have a lower $\delta^{18}O_p$ to begin with and exchange more easily with vapor at low atmospheric levels, which leads to even lower $\delta^{18}O_p$ values (Aggarwal et al., 2016). The combination of seasonality of major synoptic types and the type of rain clouds they bring therefore leads to the large seasonal amplitude of $\delta^{18}O_p$ in the South African year-round rainfall region (Fig. 7b; Braun et al., 2017).

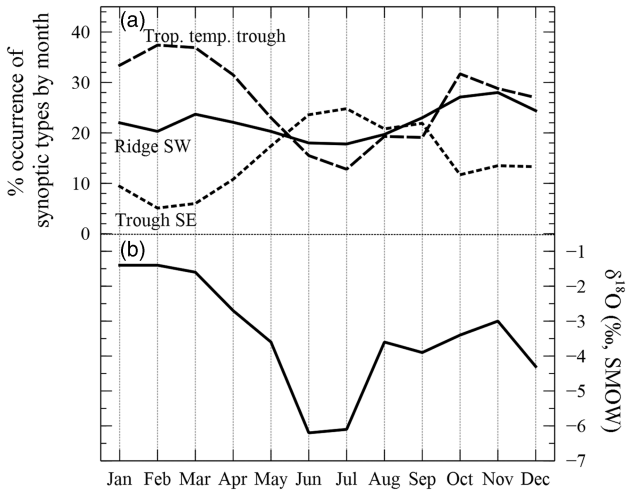

Figure 7. Monthly averages of the occurrence percentage of main circulation types (a; Engelbrecht and Landman, 2016) compared with monthly average $\delta^{18}O$ of rainfall at Mossel Bay (b; Braun et al., 2017). SMOW, standard mean ocean water.

The modern-day synoptically controlled variations in $\delta^{18}O_p$, together with the absence of evidence for cave temperature correlations with $\delta^{18}O_p$, suggest that rainfall seasonality was a major factor of $\delta^{18}O$ variation. Changes of summer insolation, equator-to-pole insolation gradients, and polar ice volume on orbital timescales bring about changes in the strength and position of the continental summer heat low, the Southern Hemisphere westerlies, and the anticyclones in the South Atlantic and South Indian Oceans (Bradley, 2015, p. 42). These variations could result in a change of the contributions of rainfall from different synoptic conditions on the south coast, which in turn would affect the $\delta^{18}O_c$ of cave speleothems through changes in $\delta^{18}O_p$. These issues will be examined in detail in the following sections, whereby, based on the modern-day pattern, shifts to higher $\delta^{18}O_c$ values will be taken to reflect a trend to more convective summer rainfall and lower $\delta^{18}O_c$ values to more stratiform winter rainfall.

Controls of the speleothem $\delta^{13}C$ values

Speleothem $\delta^{13}C$ values mainly reflect the $\delta^{13}C$ of soil CO_2 and the carbonate source material (Bredasdorp Group eolianites, calcarenites, and calcretes). In closed system conditions, where the solution is removed from contact with the soil atmosphere once it gets into contact with the carbonate source, the host rock contributes up to 50% of the carbon in the solution. However, in the porous carbonate sources in the eolianites and calcretes and the highly fractured quartzite host rock of the caves, it is likely that the solution is always in contact with the infinite reservoir of soil CO_2, which would drive the isotopic composition of the dissolved bicarbonate toward the $\delta^{13}C$ of the soil gas reservoir.

$\delta^{13}C$ values of soil CO_2 can be affected by a range of factors such as plant root respiration, microbial activity, and organic matter decay, all of which depend on the availability of water in the soil. Decrease in water availability would lead

https://doi.org/10.1017/qua.2018.61 Published online by Cambridge University Press

to reduced plant root respiration and microbial activity, as well as lower vegetation density. The $\delta^{13}C$ values of soil CO_2 would therefore shift toward higher values representative of atmospheric CO_2 rather than biogenic CO_2 (Baldini et al., 2005; Williams et al., 2005; Genty et al., 2006). Such a process is, however, most likely limited to high-latitude regions (or possibly the edges of deserts) where dramatic changes in the vegetation density lead to decreases in subsurface CO_2 concentrations to less than five times that of the atmosphere (Wong and Breecker, 2015). Furthermore, low water availability would also decrease speleothem growth rates (Genty et al., 2001), yet high $\delta^{13}C$ periods in our record (e.g., ~230–210 ka or 98–83 ka) show the coeval deposition of several speleothem samples at high temporal resolution. A reduction of water availability is also thought to cause the precipitation of calcite prior to the drip water entering the cave (prior calcite precipitation [PCP]; Fairchild et al., 2000). Effects of degassing and PCP in the bedrock are unlikely in the quartzite host rock because infiltration of the water through the dense fracture system is fast (Karkanas and Goldberg, 2010).

The alternative control of soil CO_2 $\delta^{13}C$ is vegetation type. In areas where the ranges of C3, C4, and CAM plants overlap (as on the South African south coast), changes in the proportions of these plants in the vegetation above the cave are important influences on speleothem $\delta^{13}C$ (e.g., Talma and Vogel, 1992; Holmgren et al., 2003; Bar-Matthews et al., 2010). Although C3 and C4 plants have distinct $\delta^{13}C$ values (C3: –29‰ to –22‰; C4: –16‰ to –10‰), the $\delta^{13}C$ of CAM plants can overlap with the range of C3 or C4 plants depending on whether they are obligate CAM plants (only CAM photosynthesis; $\delta^{13}C$: –10.6‰ to –18.7‰) or facultative CAM plants (possible switches between CAM and C3; $\delta^{13}C$: –16.7‰ to –27.6‰; Williams, 2015). Although CAM plants do occur in the vicinity of Pinnacle Point, they only become the dominant ground cover in the succulent karoo biome (Midgley and van der Heyden, 1999). The transition from the fynbos biome to the succulent karoo biome occurs in areas with ~200–300 mm of annual rainfall (Rebelo et al., 2006). In semiarid regions of Israel, speleothem deposition only occurs when rainfall amount exceeds 300 mm (Vaks et al., 2006). Assuming that a similar amount of annual rainfall would be required for speleothem deposition at Pinnacle Point, it is unlikely that CAM plants were a dominant proportion in the vegetation while speleothems were forming.

Another GCFR vegetation type with common, mainly facultative, CAM plants that may have colonized the cave area is subtropical thicket. The main difference between the climatic and environmental conditions of subtropical thicket and fynbos is the frequency of fires, which is much lower in thicket (Hoare et al., 2006; Rebelo et al., 2006). Low fire frequencies are found where rainfall is plenty and occurs year-round. The facultative CAM succulents in the thicket vegetation would therefore perform C3 photosynthesis (Williams, 2015), and the thicket vegetation would be indistinguishable from other C3-dominated GCFR communities.

Values of $\delta^{13}C$ of soil CO_2 therefore are changing mostly dependent on the abundance of C3 and C4 plants in the vegetation above the cave. The larger rooting depth of C3 trees compared with C4 grasses has been shown to bias the $\delta^{13}C$ in cave air CO_2 toward values representative of C3 vegetation (Wong and Breecker, 2015). Such effects are unlikely in the fynbos biome, because trees are rare (Rebelo et al., 2006) and the rooting depths are generally shallow (Higgins et al., 1987). Thicket vegetation may have considerable abundances of trees (Vlok et al., 2003); however, this vegetation type would have a dominant C3 signal also without a bias by deep roots (see Regional environment and cave formation).

Using the average measured values of $\delta^{13}C$ for C3 (–24.5‰) and C4 (–13.0‰) plants in the GCFR compiled by Williams (2015), and the enrichment factor between CO_2 and carbonate (10.35‰) from Emrich et al. (1970) and Hendy (1971) at the average present-day temperature at Mossel Bay (17.5°C; National Climatic Data Center, National Oceanic and Atmospheric Administration, 2016), pure C3 vegetation in open system conditions (constant equilibration between solutes and soil CO_2) would result in speleothem $\delta^{13}C$ of –14.2‰; in pure C4 vegetation, speleothem $\delta^{13}C$ would be –2.7‰. The boundary for mixed vegetation with 50% C3 and 50% C4 vegetation ($\delta^{13}C$ of organic matter of approximately –18.75‰) would be at –8.4‰.

In the alternative calculation for closed conditions (limited contact between infiltrating water and soil CO_2 once carbonate is being dissolved) involving stoichiometric dissolution between eolianite with marine carbonates ($\delta^{13}C$ ~ 1‰), C3 vegetation or C4 vegetation gives end member $\delta^{13}C$ values of –13.0‰ for 100‰ C3 vegetation and –4.3‰ for 100‰ C4 vegetation. In this case, the $\delta^{13}C$ of the transition from C3-dominated to C4-dominated vegetation would be –8.6‰ and thus close to the open system conditions. Carbonate in the solution in this region may, however, also originate from calcretes with $\delta^{13}C$ values between 0‰ and –8‰ (Talma and Netterberg, 1983). A combination of the marine carbonates with calcretes as the carbonate source would shift the expected $\delta^{13}C$ value for speleothems under mixed vegetation toward more negative values. However, the stoichiometric reaction model calculation is not consistent with the rapid downward penetration of solution through the host rock (Karkanas and Goldberg, 2010), which would preferentially take up the labile soil CO_2. We therefore regard the open system model to give a better approximation of the speleothem $\delta^{13}C$ values of mixed C3/C4 vegetation.

Variations of atmospheric CO_2 concentrations can affect speleothem $\delta^{13}C$ by changing the $\delta^{13}C$ values of C3 plants and by affecting their growth rate. Lower atmospheric CO_2 concentrations generally would lead to higher $\delta^{13}C$ values in the C3 plant tissue (Breecker, 2017), and the decreased growth rates caused by low atmospheric CO_2 could also cause a shift of the vegetation from C3 to C4 plants. Both these effects would lead to a negative correlation between the speleothem $\delta^{13}C$ and the concentrations of atmospheric CO_2. The $\delta^{13}C$ records from PP29 ($r = -0.20$, $P = 0.10$) and

https://doi.org/10.1017/qua.2018.61 Published online by Cambridge University Press

Staircase Cave ($r = 0.07$, $P = 0.38$) show weak correlation with atmospheric CO_2 concentration suggesting that the $\delta^{13}C$ variations we observe are not primarily caused by changes of atmospheric CO_2 but are in fact caused by changes of the vegetation composition related to other environmental drivers. Present-day distributions of C3 and C4 grasses are determined mainly by the temperature during the main rainfall season (Vogel et al., 1978; Cowling, 1983). On orbital timescales, it is also likely that the proportions of C3 and C4 plants on the south coast vary in phase with temperature and shifts in the main rainfall season. Consistent with the calculations presented previously, an increase of C4 grasses in the vegetation, which would increase speleothem $\delta^{13}C$, could be caused by either an overall increase of temperature or a shift of the rainfall seasonality toward more summer rainfall, or both. A dominance of C3 plants would be indicated by lower $\delta^{13}C$ values.

Environmental interpretation of the combined $\delta^{18}O_c$ and $\delta^{13}C$ records

To place the speleothem record within its wider regional environmental context, we address the potential connections between the $\delta^{18}O_c$ and $\delta^{13}C$ data and four other proxy records: temperature reconstructions for the Dome C ice core from Antarctica (Jouzel et al., 2007), SST reconstructions at the location of sediment core MD96-2077 on the southern border of the Agulhas Current in the Indian Ocean (Bard and Rickaby, 2009), the fraction of hemipelagic mud in sediment core MD96-2094 on Walvis Ridge (southeast Atlantic Ocean; Stuut et al., 2002), and the reconstruction of shifts of the STC from the Cape Basin record (CBR; sediment cores GeoB-3603-2 and MD96-2081; Peeters et al., 2004; Fig. 1). The hemipelagic mud on Walvis Ridge originates from nepheloid layers from the Orange River or ephemeral rivers draining the central Namib Desert and thereby is related to the amount of runoff from these rivers and rainfall amount in their drainage basins (Stuut et al., 2002). The Orange River basin covers large parts of the South African interior plateau (Fig. 1), and its runoff reflects rainfall amounts in large areas of the interior. The proximity of the STC to the CBR sites (Fig. 1) was derived by Peeters et al. (2004) using three planktonic foraminifera species: *Globorotalia inflata* and *Neogloboquadrina pachyderma* (dex.), currently occurring in waters just south of the STC, and *Globorotalia truncatulinoides*, which is found just north of it. The ratio of *G. truncatulinoides*/[*N. pachyderma* (dex.) + *G. inflata* + *G. truncatulinoides*] was used as the proxy for the STC position relative to the sediment core sites. A shift of this oceanic convergence is most likely related to a shift of the latitudinal position of the westerly winds (Bard and Rickaby, 2009).

The speleothem records and temperature proxy records are plotted together in Figure 8. Using the reasoning previously laid out for the relations of $\delta^{18}O_c$ with rainfall systems and $\delta^{13}C$ with proportions of C3 and C4 plants, we first examine the time trends in the speleothem data (Fig. 8d and e) and then how they compare with the other proxy records (Fig. 8a–c, f, and g). Our objective is to assess the correlations (or lack of) between the speleothem $\delta^{18}O_c$ and $\delta^{13}C$ series and

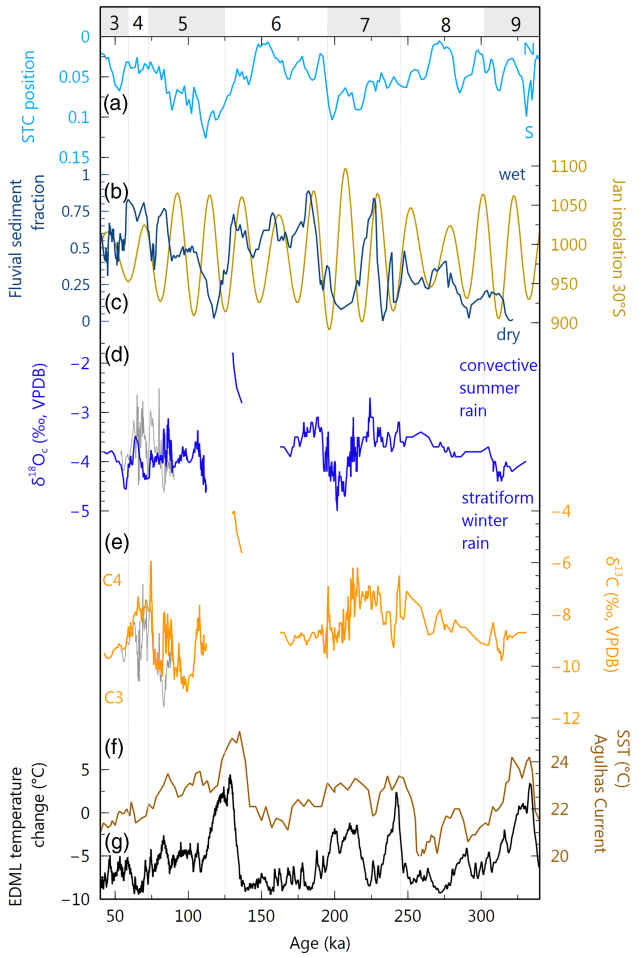

Figure 8. Comparison of the stable isotopic records from Staircase Cave and PP29 with other proxy records. (a) Reconstruction of the position of the subtropical convergence (STC) using the abundances of planktonic foraminifera found to the north and south of its present position (Peeters et al., 2004). (b) Proportion of end member 3 in the dust fraction of sediment core MD96-2094 (dark blue); this smallest size fraction originates from river runoff of the Orange River and the Central Namib Desert and reflects changes in rainfall amounts in the southern African interior (Stuut et al., 2002). (c) Summer insolation (January) at 30°S (brown; Laskar et al., 2004). (d) $\delta^{18}O_c$ of speleothems from Pinnacle Point: Staircase Cave and PP29 in blue, Crevice Cave in gray. (e) $\delta^{13}C$ of speleothems from Pinnacle Point: Staircase Cave and PP29 in orange, Crevice Cave in gray. Records of Crevice Cave from Bar-Matthews et al. (2010). (f) Sea surface temperature (SST) in the southwest Indian Ocean on the southern edge of the Agulhas Current (Bard and Rickaby, 2009). (g) Reconstruction of temperature changes relative to today at Antarctic European Project for Ice Coring in Antarctica Dronning Maud Land ice core (Jouzel et al., 2007). Numbers at the top of the figure denote Marine Oxygen Isotope Stages. VPDB, Vienna Pee Dee belemnite. (For interpretation of the references to color in this figure legend, the reader is referred to the web version of this article.)

https://doi.org/10.1017/qua.2018.61 Published online by Cambridge University Press

temperature proxy records, and the changes in the runoff of the Orange River. Correspondingly, we determine the connections between rainfall type (stratiform or convective) on the south coast with runoff from the Orange River and the position of the STC.

Modern climate and environmental conditions predict that $\delta^{18}O_c$ and $\delta^{13}C$ move in concert when rainfall seasonality and vegetation shift in phase (see the "Factors influencing the speleothem stable isotope records" section; Bar-Matthews et al., 2010). Such conditions are suggested by the covariation of $\delta^{18}O_c$ and $\delta^{13}C$ values from ~320 ka in MIS 9 to the boundary between MIS 7 and 6 at ~195 ka (Fig. 5). Thus, as the relative amount of summer rain in the form of convective rainfall increases in this interval, the abundance of C4 grasses concurrently increases and vice versa. The relationship is disturbed in the early half of MIS 6 (195–163 ka, Fig. 5), when the relative amount of convective rainfall increases, but no increase of C4 grasses is detected. After a hiatus in deposition, speleothem formation resumes between ~136 and 130 ka. In this interval at the transition from MIS 6 into MIS 5, $\delta^{18}O_c$ and $\delta^{13}C$ again follow the expected correlation (Fig. 5). This marks the end of deposition at Staircase Cave, which was likely undercut by the MIS 5e sea level high stand and collapsed. Speleothem deposition in PP29 lasted between 112 and 43 ka, but $\delta^{18}O_c$ and $\delta^{13}C$ are not correlated in this interval (Fig. 5). The contemporaneous record from Crevice Cave has higher amplitude variability and a good correlation between $\delta^{18}O_c$ and $\delta^{13}C$ (Bar-Matthews et al., 2010).

$\delta^{18}O_c$ and $\delta^{13}C$ values are low to intermediate for most of the covered period in MIS 9 and 8 suggesting overall mixed rainfall influences and vegetation. Uniform values of the speleothems in this interval might in part be related to low resolution that smooths the environmental signals. However, it appears that not even the temperature decrease from peak interglacial MIS 9 to the coldest part of MIS 8 (decrease of ~4°C of SST in MD96-2077 and decrease of ~12°C in EDML) induces a significant trend in the speleothem $\delta^{18}O_c$ and $\delta^{13}C$. Only one low of $\delta^{18}O_c$ and $\delta^{13}C$ at 312 ka deviates from the uniform values and suggests increased amounts of stratiform rainfall and C3 vegetation. This $\delta^{18}O_c$ and $\delta^{13}C$ low coincides with decreasing temperatures in Antarctica and the Agulhas Current at the transition from MIS 9 into MIS 8 (Fig. 8f and g). Low river runoff from the Orange River indicated at 318 ka (Fig. 8b) and a southward position of the westerlies at 311 ka (Fig. 8a) might also be associated with this transition period.

The termination of MIS 8 and transition into interglacial MIS 7 is characterized by increases of both $\delta^{18}O_c$ and $\delta^{13}C$ suggesting a shift toward convective summer rain and more C4 grasses. These trends coincide with steep increases of temperature in Antarctica and the Agulhas Current, as well as a short peak of rainfall amounts in the interior and intermediate north–south position of the STC and westerlies (Fig. 8a, b, f, and g). A marked drop in Antarctic temperature and Agulhas Current SST (Fig. 8f and g) after the initial peak in MIS 7 is reflected in a decrease of the $\delta^{18}O_c$ and $\delta^{13}C$ values between ~241 and 228 ka. Correspondingly, rainfall amounts in the interior are reduced (Fig. 8b), but the STC remains in an intermediate position (Fig. 8a). The second half of MIS 7 is marked by a second, longer peak of temperature in Antarctica and the Agulhas Current from ~220 to 195 ka (Fig. 8f and g). Rainfall in the interior only shows a short peak between ~230 and 220 ka, which is followed by a steep decline and low amounts until the transition into MIS 6 (Fig. 8b). The location of the STC gradually shifts to a southward position between 201 and 196 ka (Fig. 8a). The speleothem $\delta^{18}O_c$ and $\delta^{13}C$ show some differences in later MIS 7. $\delta^{18}O_c$ values follow closer with the rainfall amount suggesting a short peak of convective summer rainfall between 226 and 222 ka followed by a strong decrease and mostly stratiform rainfall between 210 and 196 ka. Values of $\delta^{13}C$ vary more in line with temperature changes with relatively high proportions of C4 plants ($\delta^{13}C > -7.5‰$) between 230 and 210 ka. Between 210 and 198 ka, vegetation shifts toward a greater proportion of C3 plants.

In early–middle MIS 6, between 195 and 163 ka, consistent $\delta^{13}C$ values of about –9‰ indicate more C3 plants than C4 grasses. Increase in $\delta^{18}O_c$ values in the same interval indicates a gradual increase of the contribution of convective summer rainfall up until ~187 ka, after which the frequency of convective rainfall declines. The temperature record from Antarctica shows a steep decrease at the transition from MIS 7 into MIS 6, and temperatures remain low throughout MIS 6 (Fig. 8g). In comparison, the SST record from the Agulhas Current shows a stepwise decline of temperatures at ~190 ka and 170 ka (Fig. 8f). Rainfall in the interior is high during MIS 6 with short peaks at 182, 158, and 131 ka. The peak at 182 ka coincides with high amounts of convective summer rain on the south coast suggested by the speleothem $\delta^{18}O_c$ values (Fig. 8b and d). The STC shows a rapid northward shift at the beginning of MIS 6 (196–190 ka) and remains in a northern to intermediate position throughout early–middle MIS 6 (Fig. 8a).

Following a hiatus, speleothem deposition in Staircase Cave resumed between 136 and 129 ka. The $\delta^{18}O_c$ and $\delta^{13}C$ values in this period are the highest for the whole record and show an increasing trend until cessation of speleothem growth. The exceptionally high values could suggest a pronounced environmental disturbance at the termination of glacial MIS 6, leading to high convective rainfall amounts and the dominance of C4 grasses. However, this time interval overlaps with the steep temperature increase at the glacial termination, a steep decrease of rainfall in the interior, and a rapid southward shift of the position of the STC (Fig. 8a, b, f, and g). This contrasts with the generally observed trends whereby high $\delta^{18}O_c$ values overlap with high runoff from the interior and an intermediate to northern position of the STC and westerlies. It should be noted that this portion of the composite record is only covered by one sample (142819), and that, despite many attempts, we have not been able to find another sample that grew at this time. The possibility therefore remains that the collapse of Staircase Cave was foreshadowed in this interval by the opening of the cave site, leading to kinetic effects and increased values of $\delta^{18}O_c$ and

https://doi.org/10.1017/qua.2018.61 Published online by Cambridge University Press

$\delta^{13}C$. The speleothem record from PP29 covers the interval between 112 and 43 ka and therefore embraces the deposition interval of the record of Crevice Cave (90–53 ka; Bar-Matthews et al., 2010). The composite record for Crevice Cave was constructed by comparing the $\delta^{18}O_c$ and $\delta^{13}C$ of all available samples and their resolutions. The samples with the highest resolution and good visual comparability to other samples were then used to construct the composite record (Bar-Matthews et al., 2010). Thus, differences in some of the details of the stable isotopic records from Crevice Cave and PP29 can be explained by the different methods used for composite record constructions. Nevertheless, the good overlap of overall trends firmly supports environmental influences as being the driving factors of these records.

During MIS 5, low $\delta^{13}C$ values of less than −7.5‰ generally suggest that C3 plants dominate the vegetation; only two intervals have values indicating mixed vegetation at ~107 ka and between 89 and 83 ka. $\delta^{18}O_c$ values show a consistent dominance of stratiform rainfall in MIS 5 with especially low values at the beginning of the PP29 record at 112 ka. Two intervals of increased contributions from convective summer rainfall are indicated at 106 and 87 ka. Both these periods coincide with peaks of SST in the Agulhas Current, whereas the Antarctic record only shows warm temperatures at 83 ka (Fig. 8f and g). Rainfall in the interior shows a distinct low between 123 and 113 ka when the STC is in a southern position (during stratiform rainfall). For the remainder of MIS 5, the interior receives intermediate rainfall amounts, except for a peak between 85 and 80 ka when the south coast received more convective summer rainfall (Fig. 8b and d). The position of the STC gradually shifts northward throughout MIS 5 (Fig. 8a). Low $\delta^{18}O_c$ and $\delta^{13}C$ values at Crevice Cave at 83 ka indicate dominant C3 vegetation and little convective rainfall.

During MIS 4, the temperature records show a clear cooling in Antarctica and the Agulhas Current. The speleothem records from PP29 and Crevice Cave suggest that there was mixed vegetation with relatively high proportions C4 grasses ($\delta^{13}C > -8$‰) and frequent convective summer rainfall. This pattern coincided with high amounts of rainfall in the interior and a northern position of the STC. In early MIS 3, low $\delta^{18}O_c$ values at PP29 suggest a short interval dominated by stratiform winter rain (59–54 ka), but this was followed by an increase in the frequency of convective systems. Stable and low $\delta^{13}C$ values suggest that C3 plants dominate the vegetation throughout the early part of MIS 3. At the same time, Antarctic temperature was stable, but Agulhas Current SST was cooling (Fig. 8f and g). Rainfall amounts in the interior are variable with intermediate values in early MIS 3 (Fig. 8b). The STC migrated from a northern to an intermediate position between 56 and 50 ka but then quickly returned north (Fig. 8a).

The time trends and comparisons described previously reveal a better compatibility of $\delta^{18}O_c$ and $\delta^{13}C$ from Pinnacle Point with rainfall amounts on the interior plateau than with temperature records from Antarctica and the Agulhas Current region. This pattern is supported by the correlation analyses of the spline smoothed records ($r = 0.55$, $P < 0.001$; Fig. 6a and c). The lack of a simple relationship with Antarctic temperature change attests to the complexities of glacial-interglacial climatic variations at the South African south coast. Our data do not support a simple model of glacial-interglacial climate change in which the northward shifted westerlies during glaciations cause an increase of winter rainfall and interglacial phases are characterized by increased summer rainfall (e.g., Van Zinderen Bakker, 1976, 1983; Chase and Meadows, 2007). Rather, we find that peaks of convective summer rainfall in early and middle MIS 7, in early MIS 6, in middle MIS 5, and during MIS 4 generally overlap with peaks of rainfall in the South African interior. Phases dominated by stratiform rainfall occur in MIS 9, at the transition from MIS 7 to MIS 6 in early MIS 5 and at the transition from MIS 4 to 3 and generally coincide with drought in the interior during phases when the STC is in a southern position. Nearly always vegetation changes track the variations in rainfall systems. Only in MIS 6 convective summer rainfall increases, but the vegetation remains dominated by C3 plants rather than showing an increased abundance of C4 grasses.

Climatic controls on orbital timescales

The speleothem $\delta^{18}O_c$ and $\delta^{13}C$ records from Pinnacle Point indicate that past climate and environments varied considerably and that these variations do not follow a simple glacial-interglacial pattern. However, summer rainfall on the South African south coast is closely connected to total rainfall on the interior plateau. The connection between the two regions is most likely related to the occurrence of tropical temperate troughs forming major cloud bands when tropical lows link up with the westerlies. Such cloud bands are a major contributor of rainfall on the interior plateau (Tyson, 1986, p. 136 ff.) and on the south coast (Engelbrecht et al., 2015). Their formation is dependent on a strong low pressure wave in the westerlies and moisture convergence in the tropics, which is favored by a strong continental heat low (Macron et al., 2014).

The position of the westerly storm tracks shifts north and south, depending on the amount of sea ice off the coasts of Antarctica (Blamey and Reason, 2007). The larger variations of Antarctic sea ice extent on orbital timescales would amplify the latitudinal migration observed under present-day conditions (e.g., Chase and Meadows, 2007). Tropical low pressure systems like the Intertropical Convergence Zone and continental heat lows over the tropical southern African interior vary their position because of the influence of precession on summer insolation. During phases of high summer insolation in the Southern Hemisphere, these low pressure systems are strengthened and shifted toward a more southern position relative to intervals with lower summer insolation (e.g., Simon et al., 2015). Figure 8 shows that peaks of summer rain on the South African south coast generally overlap with high rainfall amounts in the interior and with phases of high summer insolation.

Especially during the first half of MIS 6 and MIS 4, the south coast shows the influence of summer convective rainfall when rainfall in the interior is increased during summer

https://doi.org/10.1017/qua.2018.61 Published online by Cambridge University Press

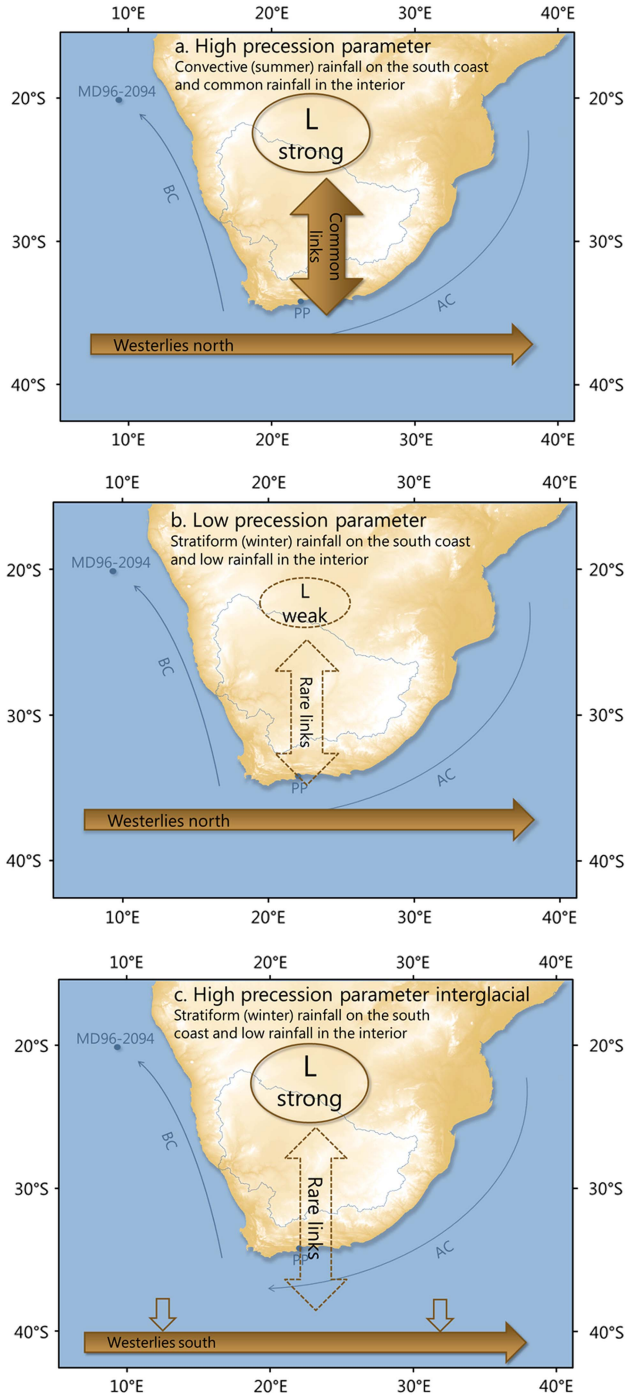

Figure 9. Schematics of the effects of shifts in the westerlies and changes in the strength of the continental heat low on the connectivity between the tropics and temperate regions. The locations of Pinnacle Point (PP) and sediment core MD96-2094, as well as the Agulhas Current (AC) and Benguela Current (BC), are indicated. Hemipelagic sediments in the core originate from the Orange River (catchment marked by blue outline). (a) Glacial high precession phase with northward-shifted westerlies and a strong continental heat low (because of high summer insolation). Convective summer rain is common on the south coast, and rainfall amount is high in the interior. (b) Glacial low precession phase, westerlies are north, but continental heat low is weak; stratiform winter rain dominates the south coast, and total rain amounts are low in the interior. (c) Interglacial high precession phase with westerlies in a southern position and strong continental heat low; stratiform winter rain dominates the south coast, and total rain amounts are low in the interior. (For interpretation of the references to color in this figure legend, the reader is referred to the web version of this article.)

insolation peaks (Fig. 8b–d). Increased Antarctic sea ice during these glacial periods probably moved the STC and westerlies northward. At the same time, peaks of Southern Hemisphere summer insolation would shift the summer heat low in the interior southward and strengthen it. The combination of these two factors leads to good connectivity between tropical and temperate low pressure systems and the frequent occurrence of tropical temperate troughs (Fig. 9a). Glacial intervals with lower precession would see a northward relocation and weakening of the continental heat low, which reduces the frequency of tropical temperate troughs, despite the maintained northern position of the westerlies (Fig. 9b).

Some of the lowest $\delta^{18}O_c$ values and highest occurrences of stratiform rainfall are observed during precession peaks in late interglacial phases. In late MIS 7 (220–190 ka), both the speleothem $\delta^{18}O_c$ and the interior rainfall record indicate low frequencies of tropical temperate troughs despite a summer insolation peak at 208 ka (Fig. 8b–d). A similar rainfall low in the interior is recorded in MIS 5 (122–112 ka) during another peak in summer insolation (116 ka). The speleothem record does not cover this second interval completely, but the record of PP29 suggests a dominance of stratiform rainfall around 112–109 ka. Both these intervals represent phases of reduced connectivity between the tropical and temperate regions, attributable to a southward shift of the STC and westerlies that is probably related to a reduction in Antarctic sea ice extent during interglacial periods (Fig. 9c).

The transition between MIS 6 and MIS 5 has the highest values of $\delta^{18}O_c$ and $\delta^{13}C$ recorded on the south coast. This suggests a steep increase of convective rainfall and C4 vegetation in an interval when rainfall in the interior was declining, the westerlies were shifting south, and summer insolation was low. This specific interval is only covered by one sample, and we therefore cannot perform the repetition test to validate the environmental significance of the stable isotope values. As noted, the high values may also be related to kinetic effects in an opening cave. The recovery of a more continuous record of this time interval in the future may help explain the exceptional values that we observe.

Implications for early modern humans and vegetation history of the GCFR

The studied speleothems derive from the same locality of two archaeological sites of major significance to modern human origins, PP13B and PP5-6 (Brown et al., 2009, 2012; Marean et al., 2007; Marean, 2010). The interpretation of the

https://doi.org/10.1017/qua.2018.61 Published online by Cambridge University Press

speleothem stable isotopic records has important implications for the reconstruction of the environmental conditions for early modern humans in the South African paleoscape and vegetation in the GCFR. Notably, it documents significant shifts in the rainfall systems and relative abundance of C3 plants and C4 grasses. Marean et al. (2014) described the main habitat types in the GCFR in terms of their major resources of interest to hunter-gatherers, and the speleothem records suggest that these habitat types changed significantly in composition and placement; they also added the Palaeo-Agulhas Plain ecosystem that formed during lower sea levels on the exposed shelf to the GCFR. Paleoenvironmental reconstructions that predate MIS 6 on the south coast are rare; we therefore focus our discussion of the paleoenvironmental implications of the speleothem record to the period from MIS 6 onward.

Despite the considerable changes in the rainfall systems indicated by variable $\delta^{18}O_c$ values during MIS 6, $\delta^{13}C$ values are relatively constant and suggest mixed vegetation with a dominance of C3 plants over C4 plants (Fig. 8e). Phytoliths from levels at PP13B dated by optically stimulated luminescence (OSL) to MIS 6 (Jacobs, 2010) also suggest a dominance of C3 plants at this time (Albert and Marean, 2012). The earliest human occupation of the caves/rock shelters at Pinnacle Point (LC-MSA Lower, 167–162 ka) was related to a short transgressive phase, when the coast was within ~5 km of the sites, in the glacial MIS 6 that was otherwise characterized by low sea levels. A slightly later MIS 6 occupation (DB Sand 4) is associated with the following regression and a wide Palaeo-Agulhas Plain (Marean et al., 2007, 2014; Fisher et al., 2010; Jacobs, 2010). The presence of large grazing ungulates typical of open grasslands and smaller taxa more characteristic for fynbos and thicket environments attests to the diverse environments that humans were using at the time, including the coast, the open grasslands of the Palaeo-Agulhas Plain, and inland areas with fynbos vegetation (Marean et al., 2007; Jerardino and Marean, 2010; Marean, 2010; Rector and Reed, 2010; Copeland et al., 2016). The mixed, but C3-dominated vegetation suggested by the speleothem $\delta^{13}C$ corresponds well with the mosaic of vegetation types indicated by the fauna. The presence of large grassland ungulates with the strong C3 signal indicated by the speleothem suggests the presence of C3 grasses during this very cold phase. Despite the increase of frequency of tropical temperate troughs, C3-dominated vegetation prevailed for most of MIS 6, possibly being favored by cooler temperatures.

The transition from MIS 6 into MIS 5 is associated with extreme climatic and environmental change. Rising sea levels rapidly flooded the entire Palaeo-Agulhas Plain removing roughly half the land surface of the present-day extent of the GCFR (Fisher et al., 2010), driving people off the plain, and obliterating the grassland ungulate populations that lived on it (Marean et al., 2014). The speleothem records may indicate a significant change in the vegetation during the transition from MIS 6 to MIS 5 with the highest abundance of C4 grasses and convective rain in the entire record (Fig. 8d and e). Micromammal assemblages from PP13B and PP9C also support a grassy environment at the end of MIS 6 (Matthews et al., 2009, 2011). The steep increase of the abundance of C4 grasses indicated by the $\delta^{13}C$ may suggest that C4 grasslands replaced fynbos biome vegetation at this time. Early MIS 5 micromammal assemblages, however, indicate a return to more closed vegetation (Matthews et al., 2009, 2011) and more favorable conditions for fynbos biome vegetation.

After the warm phase of MIS 5e, sea levels began to retreat, and the Palaeo-Agulhas Plain was again partly exposed. During MIS 5, there was a remarkable increase in the abundance of archaeological sites compared with MIS 6 (Marean et al., 2014). Large grazing ungulates, as well as intertidal shellfish, are commonly found in archaeological sites across the region (Marean et al., 2014).

A record of pollen from Vankervelsvlei near Wilderness covers the interval between 110 and 26 ka (Quick et al., 2015) and thus partly coincides with the speleothem records from Pinnacle Point. The pollen record indicated a shift from Afromontane forests in earlier MIS 5 (108–96 ka) toward forest margin and fynbos vegetation in later MIS 5 (96–70 ka; Quick et al., 2015). This shift in vegetation has been associated with climatic change from warm conditions with year-round rainfall to cooler temperatures with mainly winter rainfall (Quick et al., 2015). The speleothem records from Pinnacle Point are consistent with year-round rainfall and C3 vegetation for most of MIS 5 only with short peaks of C4 plants and summer rainfall at 106 ka and ~88 ka. The former peak coincides with a time interval when phytoliths of C4 grasses were found in PP13B (Albert and Marean, 2012). The interpretation of the Vankervelsvlei record as suggesting a cooling trend is not supported by the speleothems or phytoliths from Pinnacle Point. The archaeological deposits at Pinnacle Point suggest that hunter-gatherers expanded the use of intertidal shellfish to include variable habitats such as sandy beaches and rocky intertidal zones at this time (Jerardino and Marean, 2010; Marean, 2014; Marean et al., 2014). In the interval between 90 and 74 ka, they regularly visited PP5-6 albeit for short periods at a time (Karkanas et al., 2015).

The transition from MIS 5 to MIS 4 brought changes to the South African south coast. The pollen records from Vankervelsvlei suggest drying conditions with drought stress but without extreme conditions (Quick et al., 2015). This drying is only represented by one pollen sample in Vankervelsvlei and might not represent the whole of MIS 4. Previous paleoenvironmental interpretations from the region did not support dry conditions (Chase, 2010). At Pinnacle Point, C4 plants are abundant throughout MIS 4, and rainfall conditions are variable (Fig. 8e; Bar-Matthews et al., 2010) but with an overall increase of the connectivity between temperate and tropical regions compared with late MIS 5. Altogether, conditions seem to have been variable, and fynbos biome communities may have regularly shifted in their location during MIS 4. The constant growth of speleothem is inconsistent with conditions significantly drier than today.

https://doi.org/10.1017/qua.2018.61 Published online by Cambridge University Press

The sharp environmental change at the transition from MIS 5 into MIS 4 also marks the beginning of a series of rapid changes in stone tool technology including the introduction of a new and early microlithic technology, commitment to heat treatment of silcrete (Brown et al., 2009, 2012), and shifts in the representation of raw materials from a predominantly quartzite-based technology at the MIS 5–4 boundary to varying amounts of silcrete, quartz, and quartzite in the overlying strata (Brown, 2011). Ages of these changes are based on a high-resolution OSL age model, which is now precisely validated with the documentation of the Younger Toba tephra (~74 ka) in the PP5-6 sediments (Smith et al., 2018). The rapid innovations and technological changes thus correlate well with this period of climate variability and represent subtle adjustments to the changing environmental conditions by behaviorally modern humans (McBrearty and Brooks, 2000; Bar-Matthews et al., 2010).

The MIS 3 pollen sequence from Vankervelsvlei suggests cool conditions with increased summer aridity (Quick et al., 2015), which is supported by the higher C3 vegetation and lower convective summer rainfall amounts indicated by the Pinnacle Point speleothems.

CONCLUSIONS

We present an extended record of speleothem $\delta^{18}O_c$ and $\delta^{13}C$ from two sites at Pinnacle Point, Staircase Cave and PP29, covering the interval between 330 and 43 ka with several hiatuses. Speleothem $\delta^{18}O_c$ values are interpreted in terms of the relative contributions of rainfall from convection by tropical temperate troughs versus stratiform rainfall. $\delta^{13}C$ values of the speleothems reflect changing relative abundances of C3 plants and C4 grasses in the vegetation. More stratiform (winter) rainfall is commonly related to high abundances of C3 plants, and convective rainfall from tropical temperate troughs (summer) usually causes a spread of C4 grasses. This relationship only fails during the glacial MIS 6, when $\delta^{18}O_c$ values indicate increased convective summer rain, but vegetation remains dominated by C3 plants, probably because of cold temperatures.

Values of $\delta^{18}O_c$ in our new speleothem composite record do not support a commonly accepted model of glacial-interglacial climate change in southern Africa. The prevailing hypothesis implies a close relationship of Antarctic temperature and sea ice extent with the latitudinal position of the westerlies and the extent of the winter rainfall region. $\delta^{18}O_c$ and $\delta^{13}C$ of speleothems from Pinnacle Point do not vary in phase with temperatures in Antarctica or SST in the Agulhas Current region.

Instead, the record of $\delta^{18}O_c$ is correlated with a record of river runoff from the South African interior probably because of the high importance of tropical temperate troughs as a rainfall source in the catchment region. Peaks of river runoff and $\delta^{18}O_c$ coincide with peaks of summer (January) insolation at 30°S; only during late interglacial phases, when the STC is in a southern position, the river runoff remains low despite peaks in insolation. We therefore suggest that the occurrence frequency of tropical temperate troughs that drives changes in $\delta^{18}O_c$ and river runoff from central South Africa depends on the connectivity between the tropical summer heat low and the westerlies. High summer insolation leads to a strong continental summer heat low that connects regularly with the westerlies, whereas weaker insolation leads to a weaker heat low and lower connectivity. During strong interglacial phases, the STC and westerlies were shifted south and weakened, which also leads to decreased connectivity despite a strong summer heat low. Vegetation changes recorded by the $\delta^{13}C$ values of the speleothems follow similar trends as the $\delta^{18}O_c$ and river runoff; only during MIS 6, low temperatures may favor C3 plants, leading to low $\delta^{13}C$ values.

A comparison of the speleothem isotopic record with other indicators of past vegetation from the South African south coast shows high consistency for large parts of the record, but there are some deviations in MIS 4. Hunter-gatherers encountered variable environments in the region, with shifting vegetation and changes in the accessibility of the coast and the presence of hunting grounds on the Palaeo-Agulhas Plain related to sea levels.

ACKNOWLEDGMENTS

We thank Philip Hopley and one anonymous reviewer for their constructive comments, which helped improve this publication. We thank the Institute of Human Origins (IHO) and School of Human Evolution and Social Change (SHESC) staff at Arizona State University (ASU) and the Mossel Bay Archaeology Project (MAP) staff for their assistance, the Dias Museum for field facilities, South African Heritage Resources Agency (SAHRA) and Heritage Western Cape (HWC) for permits, and the Geological Survey of Israel for research support. We acknowledge funding from the European Commission Seventh Framework Marie Curie People program FP7/2007–2013 through funding of the Initial Training Network "GATEWAYS" (http://www.gateways itn.eu) under the grant number 238512. This research was further funded by grants from the National Science Foundation (to C.W. Marean, BCS-0524087 and BCS-1138073), the Hyde Family Foundations and the IHO at ASU, and the John Templeton Foundation to the IHO at ASU (grant ID 48952). The opinions expressed in this publication are those of the author(s) and do not necessarily reflect the views of any of these funding organizations.

REFERENCES

Aggarwal, P.K., Romatschke, U., Araguás-Araguás, L.J., Belachew, D., Longstaffe, F.J., Berg, P., Schumacher, C., Funk, A., 2016. Proportions of convective and stratiform precipitation revealed in water isotope ratios. *Nature Geoscience* 9, 624–629.

Albert, R.-M., Marean, C.W., 2012. The exploitation of plant resources by early Homo sapiens: the phytolith record from Pinnacle Point 13B Cave, South Africa. *Geoarchaeology* 27, 363–384.

Allsopp, N., Colville, J.F., Verboom, G.A., 2014. *Fynbos: Ecology, Evolution, and Conservation of a Megadiverse Region*. Oxford University Press, Oxford.

https://doi.org/10.1017/qua.2018.61 Published online by Cambridge University Press

Almogi-Labin, A., Bar-Matthews, M., Shriki, D., Kolosovsky, E., Paterne, M., Schilman, B., Ayalon, A., Aizenshtat, Z., Matthews, A., 2009. Climatic variability during the last ~90 ka of the southern and northern Levantine Basin as evident from marine records and speleothems. *Quaternary Science Reviews* 28, 2882–2896.

Baldini, J.U.L., McDermott, F., Baker, A., Baldini, L.M., Mattey, D.P., Railsback, L.B., 2005. Biomass effects on stalagmite growth and isotope ratios: a 20th century analogue from Wiltshire, England. *Earth and Planetary Science Letters* 240, 486–494.

Bard, E., Rickaby, R.E.M., 2009. Migration of the subtropical front as a modulator of glacial climate. *Nature* 460, 380–383.

Bar-Matthews, M., Ayalon, A., Gilmour, M., Matthews, A., Hawkesworth, C.J., 2003. Sea-land oxygen isotopic relationships from planktonic foraminifera and speleothems in the Eastern Mediterranean region and their implications for paleorainfall during interglacial intervals. *Geochimica et Cosmochimica Acta* 67, 3181–3199.

Bar-Matthews, M., Ayalon, A., Kaufman, A.J., 1997. Late Quaternary paleoclimate in the eastern Mediterranean region from stable isotope analysis of speleothems at Soreq Cave, Israel. *Quaternary Research* 47, 155–168.

Bar-Matthews, M., Marean, C.W., Jacobs, Z., Karkanas, P., Fisher, E.C., Herries, A.I.R., Brown, K.S., et al., 2010. A high resolution and continuous isotopic speleothem record of paleoclimate and paleoenvironment from 90-53 ka from Pinnacle Point on the south coast of South Africa. *Quaternary Science Reviews* 29, 2131–2145.

Bergh, N.G., Verboom, G.A., Rouget, M., Cowling, R.M., 2014. Vegetation types of the Greater Cape Floristic Region. In: Allsop, N., Colville, J.F., Verboom, G.A. (Eds.), *Fynbos: Ecology, Evolution, and Conservation of a Megadiverse Region*. Oxford University Press, Oxford, pp. 1–25.

Blamey, R., Reason, C.J.C., 2007. Relationship between Antarctic sea-ice and South African winter rainfall. *Climate Research* 33, 183–193.

Boch, R., Spötl, C., Kramers, J., 2009. High-resolution isotope records of early Holocene rapid climate change from two coeval stalagmites of Katerloch Cave, Austria. *Quaternary Science Reviews* 28, 2527–2538.

Bowen, G.J., 2008. Spatial analysis of the intra-annual variation of precipitation isotope ratios and its climatological corollaries. *Journal of Geophysical Research: Atmospheres* 113, 1–10.

Bradley, R.S., 2015. *Paleoclimatology: Reconstructing Climates of the Quaternary*. 3rd ed. Academic Press, Oxford.

Braun, K., Bar-Matthews, M., Ayalon, A., Zilberman, T., Matthews, A., 2017. Rainfall isotopic variability at the intersection between winter and summer rainfall regimes in coastal South Africa (Mossel Bay, Western Cape Province). *South African Journal of Geology* 120, 323–340.

Breecker, D.O., 2017. Atmospheric pCO_2 control on speleothem stable carbon isotope compositions. *Earth and Planetary Science Letters* 458, 58–68.

Brown, K.S., 2011. *The Sword in the Stone: Lithic Raw Material Exploitation in the Middle Stone Age at Pinnacle Point Site 5-6, Southern Cape, South Africa*. University of Cape Town, Cape Town.

Brown, K.S., Marean, C.W., Herries, A.I.R., Jacobs, Z., Tribolo, C., Braun, D., Roberts, D.L., Meyer, M.C., Bernatchez, J.A., 2009. Fire as an engineering tool of early modern humans. *Science* 325, 859–862.

Brown, K.S., Marean, C.W., Jacobs, Z., Schoville, B.J., Oestmo, S., Fisher, E.C., Bernatchez, J.A., Karkanas, P., Matthews, T., 2012. An early and enduring advanced technology originating 71,000 years ago in South Africa. *Nature* 491, 590–593.

Chase, B.M., 2010. South African palaeoenvironments during marine oxygen isotope stage 4: a context for the Howiesons Poort and Still Bay industries. *Journal of Archaeological Science* 37, 1359–1366.

Chase, B.M., Meadows, M.E., 2007. Late Quaternary dynamics of southern Africa's winter rainfall zone. *Earth-Science Reviews* 84, 103–138.

Cheng, H., Edwards, R.L., Shen, C.-C., Polyak, V.J., Asmerom, Y., Woodhead, J.D., Hellstrom, J.C., et al., 2013a. Improvements in ^{230}Th dating, ^{230}Th and ^{234}U half-life values, and U–Th isotopic measurements by multi-collector inductively coupled plasma mass spectrometry. *Earth and Planetary Science Letters* 371–372, 82–91.

Cheng, H., Sinha, A., Cruz, F.W., Wang, X., Edwards, R.L., D'Horta, F.M., Ribas, C.C., Vuille, M., Stott, L.D., Auler, A.S., 2013b. Climate change patterns in Amazonia and biodiversity. *Nature Communications* 4, 1411.

Chevalier, M., Chase, B.M., 2015. Southeast African records reveal a coherent shift from high- to low-latitude forcing mechanisms along the east African margin across last glacial–interglacial transition. *Quaternary Science Reviews* 125, 117–130.

Colville, J.F., Potts, A.J., Bradshaw, P.L., Measey, G.J., Snijman, D.A., Picker, M.D., Procheş, Ş., Bowie, R.C.K., Manning, J.C., 2014. Floristic and faunal Cape biochoria: do they exist? In: Allsopp, J.C., Colville, J.F., Verboom, G.A. (Eds.), *Fynbos: Ecology, Evolution, and Conservation of a Megadiverse Region*. Oxford University Press, Oxford, pp. 73–92.

Copeland, S.R., Cawthra, H.C., Fisher, E.C., Lee-Thorp, J.A., Cowling, R.M., le Roux, P.J., Hodgkins, J., Marean, C.W., 2016. Strontium isotope investigation of ingilate movement patterns on the Pleistocene Paleo-Agulhas Plain of the Greater Cape Floristic Region, South Africa. *Quaternary Science Reviews* 141, 65–84.

Cowling, R.M., 1983. The occurrence of C3 and C4 grasses in fynbos and allied shrublands in the south eastern Cape, South Africa. *Oecologia* 58, 121–127.

Cowling, R.M., Holmes, P.J., Rebelo, A.M., 1992. Plant diversity and endemism. In: Cowling, R.M. (Ed.), *The Ecology of Fynbos: Nutrients, Fire and Diversity*. Oxford University Press, Cape Town, pp. 62–112.

Cowling, R.M., Lombard, A.T., 2002. Heterogenity, speciation/extinction history and climate: explaining regional plant diversity patterns in the Cape Floristic Region. *Diversity and Distributions* 8, 163–179.

Cowling, R.M., Procheş, Ş., Partridge, T.C., 2009. Explaining the uniqueness of the Cape flora: incorporating geomorphic evolution as a factor for explaining its diversification. *Molecular Phylogenetics and Evolution* 51, 64–74.

Denniston, R.F., González, L.A., Asmerom, Y., Polyak, V.J., Reagan, M.K., Saltzman, M.R., 2001. A high-resolution speleothem record of climatic variability at the Allerød-Younger Dryas transition in Missouri, central United States. *Palaeogeography Palaeoclimatology Palaeoecology* 176, 147–155.

Dorale, J.A., Edwards, R.L., Ito, E., González, L.A., 1998. Climate and vegetation history of the midcontinent from 75 to 25 ka: a speleothem record from Crevice Cave, Missouri, USA. *Science* 282, 1871–1874.

Dorale, J.A., González, L.A., Reagan, M.K., Pickett, D.A., Murrell, M.T., Baker, R.G., 1992. A high-resolution record of Holocene climate change in speleothem calcite from Cold Water Cave, northeast Iowa. *Science* 258, 1626–1630.

https://doi.org/10.1017/qua.2018.61 Published online by Cambridge University Press

Dorale, J.A., Liu, Z., 2009. Limitations of Hendy test criteria in judging the paleoclimatic suitability of speleothems and the need for replication. *Journal of Cave and Karst Studies* 71, 73–80.

Emrich, K., Ehhalt, D.H., Vogel, J.C., 1970. Carbon isotope fractionation during the precipitation of calcium carbonate. *Earth and Planetary Science Letters* 8, 363–371.

Engelbrecht, C.J., Landman, W.A., 2016. Interannual variability of seasonal rainfall over the Cape south coast of South Africa and synoptic type association. *Climate Dynamics* 47, 295–313.

Engelbrecht, C.J., Landman, W.A., Engelbrecht, F.A., Malherbe, J., 2015. A synoptic decomposition of rainfall over the Cape south coast of South Africa. *Climate Dynamics* 44, 2589–2607.

Fairchild, I.J., Borsato, A., Tooth, A.F., Frisia, S., Hawkesworth, C. J., Huang, Y., McDermott, F., Spiro, B., 2000. Controls on trace element (Sr-Mg) compositions of carbonate cave waters: implications for speleothem climatic records. *Chemical Geology* 166, 255–269.

Fisher, E.C., Bar-Matthews, M., Jerardino, A., Marean, C.W., 2010. Middle and Late Pleistocene paleoscape modeling along the southern coast of South Africa. *Quaternary Science Reviews* 29, 1382–1398.

Fritsch, F.N., Carlson, R.E., 1980. Monotone piecewise cubic interpolation. *SIAM Journal on Numerical Analysis* 17, 238–246.

Gascoyne, M., Schwarcz, H.P., Ford, D.C., 1980. A paleotemperature record for the mid-Wisconsin in Vancouver Island. *Nature* 285, 474–476.

Genty, D., Baker, A., Vokal, B., 2001. Intra- and inter-annual growth rate of modern stalagmites. *Chemical Geology* 176, 191–212.

Genty, D., Blamart, D., Ghaleb, B., Plagnes, V., Causse, C., Bakalowicz, M., Zouari, K., et al., 2006. Timing and dynamics of the last deglaciation from European and North African δ13C stalagmite profiles-comparison with Chinese and South Hemisphere stalagmites. *Quaternary Science Reviews* 25, 2118–2142.

Goldblatt, P., Manning, J.C., 2002. Plant diversity of the Cape region of southern Africa. *Annals of the Missouri Botanical Garden* 89, 281–302.

Grant, K.M., Rohling, E.J., Bar-Matthews, M., Ayalon, A., Medina-Elizalde, M., Ramsey, C.B., Satow, C., Roberts, A.P., 2012. Rapid coupling between ice volume and polar temperature over the past 150,000 years. *Nature* 491, 744–747.

Hellstrom, J.C., Pickering, R., 2015. Recent advances and future prospects of the U–Th and U–Pb chronometers applicable to archaeology. *Journal of Archaeological Science* 56, 32–40.

Hendy, C.H., 1971. The isotopic geochemistry of speleothems—I. The calculation of the effects of different modes of formation in the isotopic composition of speleothems and their applicability as paleoclimate indicators. *Geochimica et Cosmochimica Acta* 35, 801–824.

Higgins, K.B., Lamb, A.J., van Wilgen, B.W., 1987. Root systems of selected plant species in mesic mountain fynbos in the Jonkershoek Valley, south-western Cape Province. *South African Journal of Botany* 53, 249–257.

Hoare, D.B., Mucina, L., Rutherford, M.C., Vlok, J.H.J., Euston-Brown, D.I.W., Palmer, A.R., Powrie, L.W., et al., 2006. Albany thicket biome. In: Mucina, L. Rutherford, M.C. (Eds.), *The Vegetation of South Africa, Lesotho, and Swaziland. South African National Biodiversity Institute*, Pretoria, pp. 541–567.

Holmgren, K., Lee-Thorp, J.A., Cooper, G.R.J., Lundblad, K., Partridge, T.C., Scott, L., Sithaldeen, R., Talma, A.S., Tyson, P. D., 2003. Persistent millennial-scale climatic variability over the past 25,000 years in Southern Africa. *Quaternary Science Reviews* 22, 2311–2326.

Hopley, P.J., Weedon, G.P., Marshall, J.D., Herries, A.I.R., Latham, A.G., Kuykendall, K.L., 2007. High- and low-latitude orbital forcing of early hominin habitats in South Africa. *Earth and Planetary Science Letters* 256, 419–432.

Jacobs, Z., 2010. An OSL chronology for the sedimentary deposits from Pinnacle Point Cave 13B-A punctuated presence. *Journal of Human Evolution* 59, 289–305.

Jerardino, A., Marean, C.W., 2010. Shellfish gathering, marine paleoecology and modern human behavior: perspectives from cave PP13B, Pinnacle Point, South Africa. *Journal of Human Evolution* 59, 412–424.

Jouzel, J., Masson-Delmotte, V., Cattani, O., Dreyfus, G., Falourd, S., Hoffmann, G., Minster, B., et al., 2007. Orbital and millennial Antarctic climate variability over the past 800,000 years. *Science* 317, 793–796.

Kanner, L.C., Buenning, N.H., Stott, L.D., Timmermann, A., Noone, D.C., 2014. The role of soil processes in $\delta^{18}O$ terrestrial climate proxies. *Global Biogeochemical Cycles* 28, 239–252.

Karkanas, P., Brown, K.S., Fisher, E.C., Jacobs, Z., Marean, C.W., 2015. Interpreting human behavior from depositional rates and combustion features through the study of sedimentary microfacies at site Pinnacle Point 5-6, South Africa. *Journal of Human Evolution* 85, 1–21.

Karkanas, P., Goldberg, P., 2010. Site formation processes at Pinnacle Point Cave 13B (Mossel Bay, Western Cape Province, South Africa): resolving stratigraphic and depositional complexities with micromorphology. *Journal of Human Evolution* 59, 256–273.

Lachniet, M.S., 2009. Climatic and environmental controls on speleothem oxygen-isotope values. *Quaternary Science Reviews* 28, 412–432.

Lachniet, M.S., 2015. Are aragonite stalagmites reliable paleoclimate proxies? Tests for oxygen isotope time-series replication and equilibrium. *Geological Society of America Bulletin* 127, 1521–1533.

Laskar, J., Robutel, P., Joutel, F., Gastineau, M., Correia, A.C.M., Levrard, B., 2004. A long-term numerical solution for the insolation quantities of the Earth. *Astronomy and Astrophysics* 428, 261–285.

Lutjeharms, J.R.E., 2006. *The Agulhas Current*Springer-Verlag: New York.

Macron, C., Pohl, B., Richard, Y., Bessafi, M., Macron, C., Pohl, B., Richard, Y., Bessafi, M., 2014. How do tropical temperate troughs form and develop over southern Africa? *Journal of Climatology* 27, 1633–1647.

Malan, J.A., 1990. The Stratigraphy and Sedimentology of the Bredasdorp Group, Southern Cape Province. Master's thesis, Department of Geological Sciences, University of Cape Town, Cape Town.National Climatic Data Center, National Oceanic and Atmospheric Administration.

Marean, C.W., 2010. Pinnacle Point Cave 13B (Western Cape Province, South Africa) in context: the Cape floral kingdom, shellfish, and modern human origins. *Journal of Human Evolution* 59, 425–443.

Marean, C.W., 2014. The origins and significance of coastal resource use in Africa and Western Eurasia. *Journal of Human Evolution* 77, 17–40.

Marean, C.W., 2015. An evolutionary anthropological perspective on modern human origins. *Annual Review of Anthropology* 44, 533–556.

https://doi.org/10.1017/qua.2018.61 Published online by Cambridge University Press

Marean, C.W., Bar-Matthews, M., Bernatchez, J.A., Fisher, E.C., Goldberg, P., Herries, A.I.R., Jacobs, Z., et al., 2007. Early human use of marine resources and pigment in South Africa during the Middle Pleistocene. *Nature* 449, 906–909.

Marean, C.W., Bar-Matthews, M., Fisher, E.C., Goldberg, P., Herries, A.I.R., Karkanas, P., Nilssen, P.J., Thompson, E., 2010. The stratigraphy of the Middle Stone Age sediments at Pinnacle Point Cave 13B (Mossel Bay, Western Cape Province, South Africa). *Journal of Human Evolution* 59, 234–255.

Marean, C.W., Cawthra, H.C., Cowling, R.M., Esler, K.J., Fisher, E.C., Milewski, A., Potts, A.J., Singles, E., De Vynck, J., 2014. Stone age people in a changing South African greater Cape Floristic Region. In: Allsopp, N., Colville, J.F., Verboom, G.A. (Eds.), *Fynbos: Ecology: Evolution, and Conservation of a Megadiverse Region*. Oxford University Press, Oxford, pp. 164–199.

Martínez-Méndez, G., Zahn, R., Hall, I.R., Peeters, F.J.C., Pena, L. D., Cacho, I., Negre, C., 2010. Contrasting multiproxy reconstructions of surface ocean hydrography in the Agulhas Corridor and implications for the Agulhas Leakage during the last 345,000 years. *Paleoceanography* 25, PA4227.

Matthews, T., Marean, C.W., Nilssen, P.J., 2009. Micromammals from the Middle Stone Age (92–167 ka) at Cave PP13B, Pinnacle Point, south coast, South Africa. *Palaeontologia Africana* 44, 112–120.

Matthews, T., Rector, A.L., Jacobs, Z., Herries, A.I.R., Marean, C. W., 2011. Environmental implications of micromammals accumulated close to the MIS 6 to MIS 5 transition at Pinnacle Point Cave 9 (Mossel Bay, Western Cape Province, South Africa). *Palaeogeography, Palaeoclimatology Palaeoecology* 302, 213–229.

McBrearty, S., Brooks, A.S., 2000. The revolution that wasn't: a new interpretation of the origin of modern human behavior. *Journal of Human Evolution* 39, 453–563.

McDermott, F., 2004. Paleo-climate reconstruction from stable isotopic variations in speleothems: a review. *Quaternary Science Reviews* 23, 901–918.

Mickler, P.J., Stern, L.A., Banner, J.L., 2006. Large kinetic isotope effects in modern speleothems. *GSA Bulletin* 118, 65–81.

Midgley, G.F., van der Heyden, F., 1999. Form and function in perennial plants. In: Dean, W.R.J., Milton, S.J. (Eds.), *The Karoo: Ecological Patterns and Processes*. Cambridge University Press, Cambridge, pp. 91–106.

Mucina, L., Rutherford, M.C., 2006. *The Vegetation of South Africa, Lesotho, and Swaziland. Strelitzia 19*. South African National Biodiversity Institute: Pretoria.

National Climatic Data Center, National Oceanic and Atmospheric Administration. 2016. Global Surface Summary of the Day (accessed September 9, 2016). https://gis.ncdc.noaa.gov/maps/ncei.

Oster, J.L., Montañez, I.P., Santare, L.R., Sharp, W.D., Wong, C., Cooper, K.M., 2015. Stalagmite records of hydroclimate in central California during termination 1. *Quaternary Science Reviews* 127, 199–214.

Peeters, F.J.C., Acheson, R., Brummer, G.-J.A., de Ruijter, W.P.M., Schneider, R.R., Ganssen, G.M., Ufkes, E., Kroon, D., 2004. Vigorous exchange between the Indian and Atlantic oceans at the end of the past five glacial periods. *Nature* 430, 661–665.

Poage, M.A., Chamberlain, C.P., 2001. Empirical relationships between elevation and the stable isotope composition of precipitation and surface waters: considerations for studies of paleoelevation change. *American Journal of Science* 301, 1–15.

Quick, L.J., Meadows, M.E., Bateman, M.D., Kirsten, K.L., Mäusbacher, R., Haberzettl, T., Chase, B.M., 2015. Vegetation and climate dynamics during the last glacial period in the fynbos-afrotemperate forest ecotone, southern Cape, South Africa. *Quaternary International* 404, 136–149.

R Core Team. 2017. R: A language and environment for statistical computing. https://www.r-project.org/.

Rebelo, A.G., Boucher, C., Helme, N., Mucina, L., Rutherford, M. C., 2006. Fynbos biome. In: Mucina, L., Rutherford, M.C. (Eds.), *The Vegetation of South Africa, Lesotho, and Swaziland. Strelitzia 19*. South African National Biodiversity Institute, Pretoria pp. 52–219.

Rector, A.L., Reed, K.E., 2010. Middle and late Pleistocene faunas of Pinnacle Point and their paleoecological implications. *Journal of Human Evolution* 59, 340–357.

Rohling, E.J., Grant, K.M., Bolshaw, M., Roberts, A.P., Siddall, M., Hemleben, C., Kucera, M., 2009. Antarctic temperature and global sea level closely coupled over the past five glacial cycles. *Nature Geoscience* 2, 500–504.

Rozanski, K., Araguás-Araguás, L.J., Gonfiantini, R., 1993. Isotopic patterns in modern global precipitation. In: Swart, P.K. Lohmann, K.C., McKenzie, J., Savin, S. (Eds.), *Climate Change in Continental Isotopic Records*. American Geophysical Union, Washington, D.C., pp. 1–36.

Scholz, D., Hoffmann, D.L., 2011. StalAge – an algorithm designed for construction of speleothem age models. *Quaternary Geochronology* 6, 369–382.

Schulze, B.R., 1972. South Africa. In: Groffiths, J.F. (Ed.), *Climates of Africa. World Survey of Climatology*. Elsevier: Amsterdam, pp. 501–566.

Scott, L., Neumann, F.H., Brook, G.A., Bousman, C.B., Norström, E., Metwally, A.A., 2012. Terrestrial fossil-pollen evidence of climate change during the last 26 thousand years in Southern Africa. *Quaternary Science Reviews* 32, 100–118.

Simon, M.H., Ziegler, M., Bosman, J., Barker, S., Reason, C.J.C., Hall, I.R., 2015. Eastern South African hydroclimate over the past 270,000 years. *Nature Geoscience Reports* 5, 18153.

Smith, E.I., Jacobs, Z., Johnsen, R., Ren, M., Fisher, E.C., Oestmo, S., Wilkins, J., et al., 2018. Humans thrived in South Africa through the Toba eruption about 74,000 years ago. *Nature* 555, 511–515.

Stríkis, N.M., Cruz, F.W.J., Cheng, H., Karmann, I., Edwards, R.L., Vuille, M., Wang, X., de Paula, M.S., Novello, V.F., Auler, A.S., 2011. Abrupt variations in South American monsoon rainfall during the Holocene based on a speleothem record from central-eastern Brazil. *Geology* 39, 1075–1078.

Stuut, J.-B.W., Prins, M.A., Schneider, R.R., Weltje, G.J., Jansen, J. H.F., Postma, G., 2002. A 300-kyr record of aridity and wind strength in southwestern Africa: inferences from grain-size distributions of sediments on Walvis Ridge, SE Atlantic. *Marine Geology* 180, 221–233.

Talma, A.S., Netterberg, F., 1983. *Stable isotope abundances in calcretes. Geological Society*, London, Special Publications 11, 221–233.

Talma, A.S., Vogel, J.C., 1992. Late Quaternary paleotemperatures derived from a speleothem from Cango Caves, Cape Province, South Africa. *Quaternary Research* 37, 203–213.

Theron, J.N., Malan, J.A., Hill, R.S., 1989. *Lithostratigraphy of the Skurweberg Formation (Table Mountain Group). South African Committee for Stratigraphy, Lithostratigraphic Series 3*. Govenrnment Printer, Pretoria.

https://doi.org/10.1017/qua.2018.61 Published online by Cambridge University Press

Todd, M.C., Washington, R., 1999. Circulation anomalies associated with tropical-temperate toughs in southern Africa and the south west Indian Ocean. *Climate Dynamics* 15, 937–951.

Tyson, P.D., 1986. *Climatic Change and Variability in Southern Africa*. Oxford University Press: Cape Town.

Tyson, P.D., Preston-Whyte, R.A., 2000. *The Weather and Climate of Southern Africa*. Oxford University Press, Oxford.

Vaks, A., Bar-Matthews, M., Ayalon, A., Matthews, A., Frumkin, A., Dayan, U., Halicz, L., Almogi-Labin, A., Schilman, B., 2006. Paleoclimate and location of the border between Mediterranean climate region and the Saharo–Arabian Desert as revealed by speleothems from the northern Negev Desert, Israel. *Earth and Planetary Science Letters* 249, 384–399.

Vaks, A., Bar-Matthews, M., Matthews, A., Ayalon, A., Frumkin, A., 2010. Middle-Late Quaternary paleoclimate of northern margins of the Saharan-Arabian Desert: reconstruction from speleothems of Negev Desert, Israel. *Quaternary Science Reviews* 29, 2647–2662.

Van Zinderen Bakker, E.M., 1976. The evolution of Late Quaternary palaeoclimates of southern *Africa. Palaeoecology of Africa* 9, 160–202.

Van Zinderen Bakker, E.M., 1983. The Late Quaternary history of climate and vegetation in East and southern Africa. *Bothalia* 14, 369–375.

Van Zinderen Bakker, E.M., Illies, J., 1978. Quaternary vegetation changes in southern Africa. In: Werger, M.J.A. (Ed.), *Biogeography and Ecology of Southern Africa*, Springer, The Hague, the Netherlands, pp. 131–143.

Vlok, J.H.J., Euston-Brown, D.I.W., Cowling, R.M., Hoffman, M. T., 2003. Acocks' Valley Bushveld 50 years on: new perspectives on the delimitation, characterisation and origin of subtropical thicket vegetation. *South African Journal of Botany* 69, 27–51.

Vogel, J.C., Fuls, A., Ellis, R.P., 1978. The geographical distribution of Kranz grasses in South Africa. *South African Journal of Science* 74, 209–215.

Wadley, L., 2015. Those marvellous millennia: the Middle Stone Age of southern Africa. *Aznia: Archaeological Research in Africa* 50, 155–226.

Wilkins, J., Brown, K.S., Oestmo, S., Pereira, T., Ranhorn, K.L., Schoville, B.J., Marean, C.W., 2017. Lithic technological responses to Late Pleistocene glacial cycling at Pinnacle Point Site 5-6, South Africa. *PLoS ONE* 12, e0174051.

Williams, H.M., 2015. Stable Isotope Analysis of Archaeological and Modern Micromammals from the Greater Cape Floristic Region near Pinnacle Point, on the South Coast of South Africa. PhD dissertation, Arizona State University, Tempe.

Williams, P.W., King, D.N.T., Zhao, J., Collerson, K.D., 2005. Late Pleistocene to Holocene composite speleothem ^{18}O and ^{13}C chronologies from South Island, New Zealand—did a global Younger Dryas really exist? *Earth and Planetary Science Letters* 230, 301–317.

Willis, C.K., Cowling, R.M., Lombard, A.T., 1996. Patterns of endemism in the limestone flora of South African lowland fynbos. *Biodiversity Conservation* 5, 55–73.

Winnick, M.J., Chamberlain, C.P., Caves, J.K., Welker, J.M., 2014. Quantifying the isotopic "continental effect. *Earth and Planetary Science Letters* 406, 123–133.

Wong, C.I., Breecker, D.O., 2015. Advancements in the use of speleothems as climate archives. *Quaternary Science Reviews* 127, 1–18.

https://doi.org/10.1017/qua.2018.61 Published online by Cambridge University Press